Cyclone generation Algorithm including a THERmodynamic module for Integrated National damage Assessment (CATHERINA 1.0) compatible with CMIP climate data

Théo Le Guenedal[1], Philippe Drobinski[2], and Peter Tankov[1]

[1]CREST, ENSAE, Institut Polytechnique de Paris, Palaiseau, France
[2]LMD-IPSL, Ecole Polytechnique, Institut Polytechnique de Paris, ENS, PSL Research University, Sorbonne Université, CNRS, Palaiseau, France

Correspondence: Theo Le Guenedal (theo.le-guenedal@ensae.fr)

Abstract. Tropical cyclones are responsible for a large share of global damage resulting from natural disasters and estimating cyclone-related damage at a national level is a challenge attracting growing interest in the context of climate change. The global climate models, whose outputs are available from the Coupled Model Intercomparison Project (CMIP), do not resolve tropical cyclones. The Cyclone generation Algorithm including a THERmodynamic module for Integrated National damage Assessment (CATHERINA) presented in this paper, couples statistical and thermodynamic relationships to generate synthetic tracks sensitive to local climate conditions and estimates the damage induced by tropical cyclones at a national level. The framework is designed to be compatible with ~~CMIP models data offering a simple~~ the data from CMIP models offering a reliable solution to resolve tropical cyclones in climate projections. We illustrate ~~it~~ this by producing damage projections in Representative Concentration Pathways (RCP) at the global level and for individual countries. The algorithm contains a module to correct biases in climate models based on the distributions of the climate variables in the reanalyses. This model was primary developed to answer the need of the economic and financial community that is seeking quantitative signals that would allow for a better quantification of physical risks in the long term, to estimate, for example, the impact on sovereign debt.

1 Introduction

Climate-related physical risks pose a growing threat to humanity, and the design and implementation of adequate adaptation and mitigation measures require assessing future physical risks at a national and global scale. ~~One~~ The projections of the global climate models are an important source of information about the future climate~~are the projections of the global climate models, however~~. However, the spatial resolution of these global models is unfortunately still not sufficient to fully resolve extreme events, particularly tropical cyclones. On the other side of the spectrum, Integrated Assessment Models (IAM) directly assess the impact of the climate on economic activity. ~~Most of these models~~ Although these models are used to calibrate optimal mitigation or adaptation pathways, most of them embed a physical damage module, usually limited to a very generic damage function. Tools to assess the impact of ~~tropical cyclones on the economy under future climate are thus lacking~~ future cyclones in shared socioeconomic pathways are starting to appear in the literature. For example Geiger et al. (2021) evaluate the population

exposure. Our study instead focuses on the damage costs of tropical cyclones with the aim to include these advanced signals in integrated economic modeling. The objective of this paper is to fill ~~this gap : we~~ the gap between climate models and integrated assessments: We build synthetic cyclones based on the climate data produced by the global climate models, and evaluate the economic damage of these synthetic cyclones under ~~various assumptions~~ assumptions regarding the socio-economic scenarios.

The physics of tropical cyclones has been intensively studied in the literature. The thermodynamic cyclone theory builds upon the seminal contributions by Emanuel (1988) followed by Holland (1997) and Emanuel (1999). Concerning the impact of climate change, it is well known that the presence of greenhouse gases in the atmosphere increases the radiative forcing, which leads to a progressive warming of the atmosphere (Butchart et al., 2000), and the rise of sea surface temperatures (Solomon et al., 2007; Pachauri et al., 2014). This phenomenon increases the amount of energy available for cyclones to grow in intensity (Emanuel, 1991) and this growth is already measurable (Emanuel, 2005). Risk assessments have been developed based on hurricane potential intensity maps to assess the damage in the US and ~~worldwide~~ around the world (Emanuel et al., 2008; Emanuel, 2011; Mendelsohn et al., 2012).

Models relying on statistical relationships (James and Mason, 2005; DeMaria and Kaplan, 1994; Kaplan and DeMaria, 1995) are available in the literature to produce synthetic cyclones with properties closely resembling those of observed cyclones. Recently, ~~Bloemendaal et al. (2020)~~ Bloemendaal et al. (2020) developed a modeling framework to simulate realistic synthetic tropical cyclone tracks: the Synthetic Tropical cyclOnes geneRation Model (STORM). ~~However,~~ This model computes the maximum pressure intensity (MPI) associated with the sea-surface temperature (SST), and uses this potential as a predictor in the central pressure dynamics (James and Mason, 2005). In line with Merrill (1987), we find that ~~the~~ although the sea-surface temperature plays a major role, this variable alone is not a reliable predictor of whether a given storm will intensify. Thus, we prefer to rely on the formulation of Holland (1997) and model the effect of climate change on the maximum potentials in the different scenarios ~~can only be modeled by~~ through a better description of the underlying thermodynamic phenomenon, well described by Emanuel (1988); Holland (1997) or Emanuel (1999). We therefore develop an alternative to STORM by adding a thermodynamic module in the perspective of producing cyclones in different climate scenarios. In particular, we retrieve two additional variables (relative humidity and tropopause temperature) from climate models to ~~better describe the intensification process~~bridge the gap between data from global circulation models (GCMs) and the theory of the intensification of tropical depressions.

On the damage modeling side, Bresch (2017); Lüthi (2019); Aznar Siguan and Bresch (2019) set up a platform for physical risk estimation (CLIMADA), coupled with a database of estimated values of local assets (Eberenz et al., 2019, 2020). The asset resolution (30 arc-sec) and geo-spatial description of extreme events is particularly advanced. We propose a simplification of this work that applies in the context of national level assessment. The CLIMADA framework focuses on damage modeling based on ~~simplified climate projections ,~~ global aggregated temperature projections and does not make use of the climate data produced by ~~AOCGM. Coupling~~ atmosphere-ocean general circulation models (AOGCM). Coupling CLIMADA and STORM methodology with ~~our original~~ an extended thermodynamic module fitted on four climate variables~~and CLIMADA~~, our approach provides a ~~better~~ novel long-term tail risk assessment at a national level, ~~and therefore a better measure of the adaptation investments needed~~ offering an adaptive framework to estimate investments required to mitigate this risk.

This paper makes three contributions. First, we provide an algorithm to generate synthetic cyclones from climate data inspired by Bloemendaal et al. (2020) fitted on four physical variables extracted from ERA-5 reanalysis and including a thermodynamic module to better describe cyclone physics. Second, we ~~ensure that this algorithm is compatible with~~ build an algorithm generating synthetic tracks directly from CMIP models, expose the biases in CMIP5 datasets and propose a correction module based on Vrac et al. (2012). Third, we bridge the gap between climate data and damage modeling by using the physical asset values from Eberenz et al. (2020) and computing the damage along cyclone tracks using the regional specific damage functions designed in the CLIMADA project. Combining open data sources and methodologies allows us to propose a complete bottom-up integrated physical ~~risks~~ risk assessment model for tropical cyclones presented in Figure 1: the Cyclone generation Algorithm including a THERmodynamic module for Integrated National damage Assessment (CATHERINA).

The process is the following. The cyclones are initiated with spatial and seasonal distribution estimated on the IBTrACS database similarly to Bloemendaal et al. (2020). Their movement is described with a simple auto regressive stochastic process (James and Mason, 2005; Bloemendaal et al., 2020). Along the simulated cyclone tracks, we retrieve climate variables from climate models allowing to define locally the maximum potential intensity based on the simplified expression in Holland (1997). Some controls such as the maximum pressure drop observed for the corresponding temperature and the decay relationship for cyclones evolving over land are also fitted for each basin and applied in the synthetic tracks generation algorithm. Extracting the climate variables from different models allows us to correct the biases and evaluate model uncertainty. Then, we use the physical asset values (Eberenz et al., 2020) and regional damage functions from the CLIMADA module to evaluate the cyclone-related damage at a national level. This step requires to extract the local physical asset values and aggregate them on tiles of length defined proportionally to the average radius to maximum wind (approx. $50\mathrm{km}$) along the cyclone path. Summing the losses along tracks for each year and for each country allows us to establish a national assessment of the damage generated by tropical cyclones.

CATHERINA aims to provide country-level estimates for the future damage from tropical cyclones, consistent with climate model projections, with mainly economic and financial applications in mind. Examples of applications include estimating the impact of cyclones on the creditworthiness of government debt; providing a physical risk module for integrated assessment models; creating physical risk scenarios for stress testing the resiliency of the financial system at a country level and at a global level etc. Given this aggregate country-level analysis objective, our model is certainly a simplification compared to state-of-the-art cyclone dynamics models, does not aim for precise prediction of individual cyclone tracks, and does not integrate a bottom-up description of damage to individual assets. At the same time, our paper improves earlier studies of cyclone damage on the aggregate level. For example, compared to Mendelsohn et al. (2012): our model uses several climate scenarios with state-of-the-art bias correction, as well as Shared Socioeconomic Pathways (SSPs) to project population and regional domestic products and is based on precise physical asset value distribution.

The paper is organized as follows. Section 2 describes the datasets used to fit the model on ERA-5 and to generate synthetic cyclones based on both ERA-5 and CMIP5 models datasets. Section 3 describes the statistical calibration process and the details of the thermodynamic instrumental variables. Section 4 recalls the calibration methods implemented in the CLIMADA environment to fit the regional damage functions, defines the parameters of these functions using Eberenz et al. (2021) and

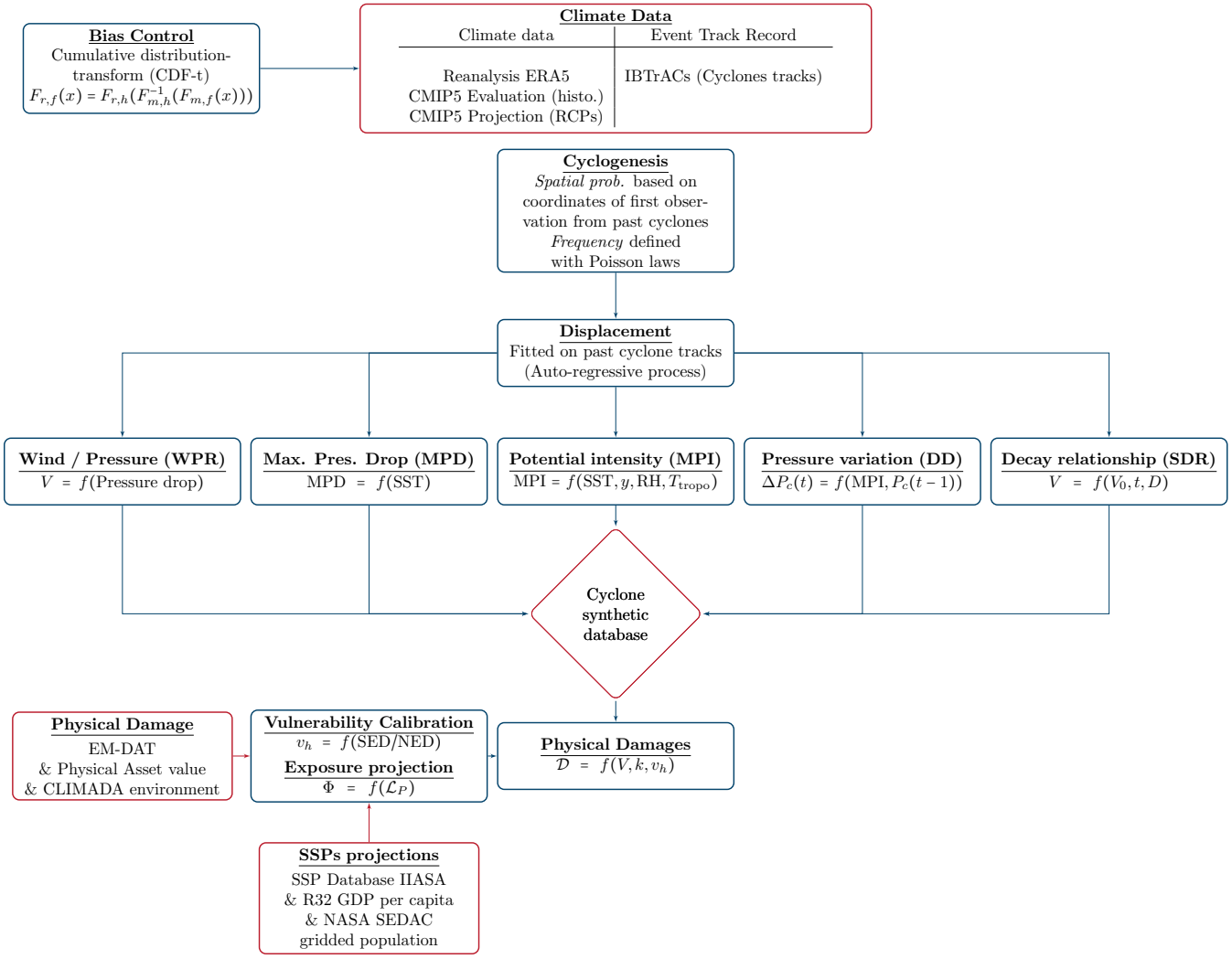

Figure 1. Cyclone generation Algorithm including a THERmodynamic module for Integrated National damage Assessment (CATHERINA) Framework

applies them along the synthetic tracks produced to study the distribution of national annual damages. Section 5 explores the properties of the produced synthetic tracks, with ERA-5 and 7 CMIP models, assesses climate uncertainty and introduces the bias correction module in the context of changing climate conditions. To close this section, we present the global and regional projections of cyclone damage between 2070 and 2100 obtained with CATHERINA.

2 Input data

In the CATHERINA framework, we fit the properties of historical cyclones (IBTrACS database) on past climate reanalyses (ERA-5) in the perspective of describing future cyclones based on global climate models outputs (CMIP), having a lower spatial and temporal resolution. This perspective constrains us to use monthly data.

2.1 Climate model data (CMIP)

CATHERINA aims at generating ~~cyclones~~ cyclone tracks with properties drawn from climate models to enable national damage assessments, bridging the gap between Atmosphere-Ocean General Circulation Models (AOGCM) outputs and damage assessments. To reduce the bias in the variables produced by climate models [1] and evaluate the performance of CATHERINA on past data by comparing the simulated cyclone damages to the realized ones we use historical simulations (as opposed to future climate projections) from the Coupled Model Inter-comparison project (Phase 5) models (Taylor et al., 2012). We use the historical climate simulations at the monthly frequency for the relative humidity (RH) at two meters, sea surface temperature (SST), mean sea level pressure (MSLP) and tropauspose temperature (~~T_{tropo}~~ T_{tropo}) (at pressure level of 50 hPa) from Copernicus climate data store[1] ~~.~~.[1] CMIP5 data are used in the 5th assessment report of the Intergovernmental Panel on Climate Change (IPCC). The latest synthesis Report in ~~progress in 2021 is~~ 2022 (IPCC AR6[2] ~~, which~~) uses CMIP6 datasets but in the present paper, we use CMIP5 data because of the broader availability of climate variables.

We use models from the following climate centers: NASA, Goddard Institute for Space Studies (GISS-E2-H, USA), Institut Pierre Simon Laplace (IPSL-CM5A-NR, France), Bureau of Meteorology - Commonwealth Scientific and Industrial Research Organisation (ACCESS1-0, BoM-CSIRO, Australia), ~~Beijin~~ Beijing Climate Center (bcc-csm1-1-m, China), Institute of Numerical Mathematics (inmcm4, Russia), Norwegian Climate Centre (NorESM1-ME, Norway), Canadian Centre for Climate Modelling and Analysis (CanESM2, Canada). The spatial resolution goes from 0.75° to 2.5° depending on the model (See Table 1). Each climate model produces a potentially biased estimate of multiple climate variables at the spatial resolution given in Table 1 and on a monthly basis. The choice of the CGMs was driven by the availability of the variables of interest in the Copernicus Climate data store (CDS) in the representative concentration pathways used in the exercise (RCP 2.6, 4.5 and 8.5 W/m2) in both single level and multiple pressure level monthly data in the same ensemble (r1i1p1). We also aimed at having multiple regions represented.

To reduce the influence of ~~these biases~~model bias, we use a large number of models and consider the distribution of results provided by all the models. Then we correct, variable by variable, and for each basin ~~,~~ and each model, the biases with respect to the reanalysis along the same tracks.

[1] ~~In particular, we need the climate variables produced by climate models on a time period covered by reanalysis (cf. section 2.2) to define the bias correction functions (cf. section 5.1).~~

[1] ~~Climate data is available on the Copernicus Climate data store: .~~

[1] Climate data is available on the Copernicus Climate data store: https://cds.climate.copernicus.eu/.

[2] ~~.~~

Table 1. Climate data resolution

	Resolution (x, y) in degrees
ERA-5 (Reanalysis)	0.25 x 0.25
ACCESS1-0 (BoM-CSIRO, Australia)	1.875x 0.9331648
CanESM2 (CCCMA, Canada)	1.40625 x 0.9364358
GISS-E2-H (NASA, USA)	2.5 x 2
NorESM1-ME (NCC, Norway)	1 x 1
bcc-csm1-1-m (BCC, China)	1 x 0.7402597
IPSL-CM5A-MR (IPSL, France)	1 x 1
INMCM4 (INM, Russia)	2 x1.5

2.2 ERA-5 Reanalysis

Climate reanalyses describe the historical climate conditions, obtained by assimilating all available observations into the models. They provide numerical estimates of atmospheric parameters (e.g. air temperature, pressure and wind) at different altitudes / pressure levels, and surface parameters (such as rainfall, soil moisture content, ocean-wave height and sea-surface temperature) on a single level. We use reanalyses to calibrate the cyclone generation algorithm based on the most realistic available estimates of climate variables.

We use ERA-5 reanalysis from the European Centre for Medium-Range Weather Forecasts (ECMWF) to fit the CATHERINA model[2] (Hersbach et al., 2020). This dataset covers the Earth on a 30 km grid (~ 0.25 °) and resolves the atmosphere using 137 levels from the surface up to a height of 80 km. In this paper, to ensure compatibility with CMIP5 models, we extract mean ~~sea level~~ sea-level pressure (MSLP), ~~sea surface~~ sea-surface temperature (SST), ~~sea level~~ sea-level relative humidity (RH), and tropopause temperature (T_{tropo}) at the monthly frequency. Because ERA-5 better resolves past tropical cyclones than climate models, the historical mean ~~sea level~~ sea-level pressure values in ERA-5 are influenced by their presence. Consequently, we retrieve the mean ~~sea level pressure~~ sea-level pressure and environmental relative humidity 500 km ($\sim 5°$ longitude) away from the storm center to extract a value for P_{env}, that is meant to represent the pressure - at a given latitude and season - in normal environmental conditions.[3]

[2]Climate data is available on the Copernicus Climate data store: https://cds.climate.copernicus.eu/.

[3]We retrieve both pressure (MSLP) and humidity (RH) to define P^{env} and RH^{env} (Holland, 1997) away from the center in the reanalysis because tropical cyclone thermodynamic potential intensity - through thermodynamic efficiency and moist entropy (Equation (8) and (7))- arise from the deviations from the normal conditions. Monthly averaging may smooth values so that the data extracted along historical tracks may not represent the conditions at the time of cyclone passage. Therefore, using monthly means, this translation is mainly made for reasons of theoretical coherence. In future studies, this model will be applied with higher temporal resolution and performing this translation would be more important. In the present version of our paper, because the CMIP5 projections of the sea-level temperature were only available at monthly frequency in the CDS, we chose to perform the exercise using monthly data to illustrate our approach.

2.3 Historical cyclone tracks (IBTrACS)

We use the International Best Track Archive for Climate Stewardship (IBTrACS) database (Knapp et al., 2010)[4]~~.~~.[4] This database provides information on past cyclone tracks at 3-hour frequency. We remove the events classified as disturbance or extra tropical, and do not consider the South Atlantic basin [5](see Figures A1 for more information). Climate reanalysis availability requires us to focus on ~~cyclones since~~ post 1980 cyclones, which reduces the database to ~~4 411~~ 4,574 cyclones. In the context of an integrated damage assessment, to focus on the events that have a potentially substantial impact on assets, we select only tropical cyclones with maximum wind speed exceeding 35 $\mathrm{m.s}^{-1}$ obtaining ~~2 245 cyclones .~~ 2,966 on the full database and 1,451 focusing on tropical cyclones between 1980 and April 2020. In Figure 2, we plot the central pressure along each cyclone life. This graph suggests that the cyclone phases are fully represented in the database i.e. from the genesis to dissipation. ~~The trajectories of central pressure in the~~ The North Indian basin ~~appear more erratic, which means that we can expect to obtain less significant relationships in this basin. Specific examples of the evolution of central pressure and wind are given in Figure ?? for some famous named cyclones in the North Atlantic basin .~~ has the lowest number of reported events with wind speed above 35 $\mathrm{m.s}^{-1}$ (50 compared to 291 for East Pacific, 185 for North Atlantic, 305 for South Indian, 158 for South Pacific and 515 for West Pacific) with variable reporting quality, which explains the more erratic shapes of the central pressure. For example, the return to normal of some events does not seem to be completely reported for this basin as indicated in Figure 2. We extract the maximum wind speed, cyclone eye pressure and coordinate variations of the eye from this database.

2.4 Physical asset exposure and damage

Eberenz et al. (2019) present a methodology to downscale physical asset values on a high-resolution grid using a combination of nightlight intensity, population data, and global country indicators and make their dataset fully available (Eberenz et al., 2020). These estimates of physical asset value are based on the light intensity L_i – from Nighttime lights of the Black Marble 2016 annual composite of the VIIRS day–night band (DNB) (Román et al., 2018) in 2016 at the 15 arc-second resolution – and the population P_{pix} per pixel – from Gridded Population of the World (GPW) database (Center for International Earth Science Information Network (CIESIN), 2017) in 2015 at the 30 arc-sec resolution for 224 countries, and various additional sources[5] allowing to define the total asset (A_{tot}) for each country. This value is distributed to each grid cell proportionally to the light intensity L_i times the local population P_{pix}[6]~~.~~

$$A_{pix} = A_{tot} \frac{L_i \cdot P_{pix}}{\sum_{pix_i}^{N} (L_i \cdot P_{pix_i})}.$$

[4] ~~See for a browser of the data and for the full dataset.~~

[4] See http://ibtracs.unca.edu/ for a browser of the data and https://www.ncdc.noaa.gov/ibtracs/index.php?name=ib-v4-access for the full dataset.

[5] ~~See Figure A1 and ?? on page 45 for more information.~~

[5] Produced Capital, comprehensive global estimate of produced capital stock, i.e. the value of produced or manufactured assets per country (World Bank, 2018) – 2014 / 140 countries; the GDP to wealth ratio from Global Wealth Report ~~(Credit Suisse Research Institute, 2017)~~ (Credit Suisse, 2017) – 2017 / 84 countries; the gross domestic product (GDP) per country from World Bank Open Data portal ~~(World Bank, 2019b)~~ (World Bank, 2019) – 2014 / 224 countries and Subnational equivalent of GDP (GRP) from varying sources – 2012-2017 / 504 regions in 14 countries.

[6] ~~The values of A_{pix} on a 30 arc-second grid are available at .~~

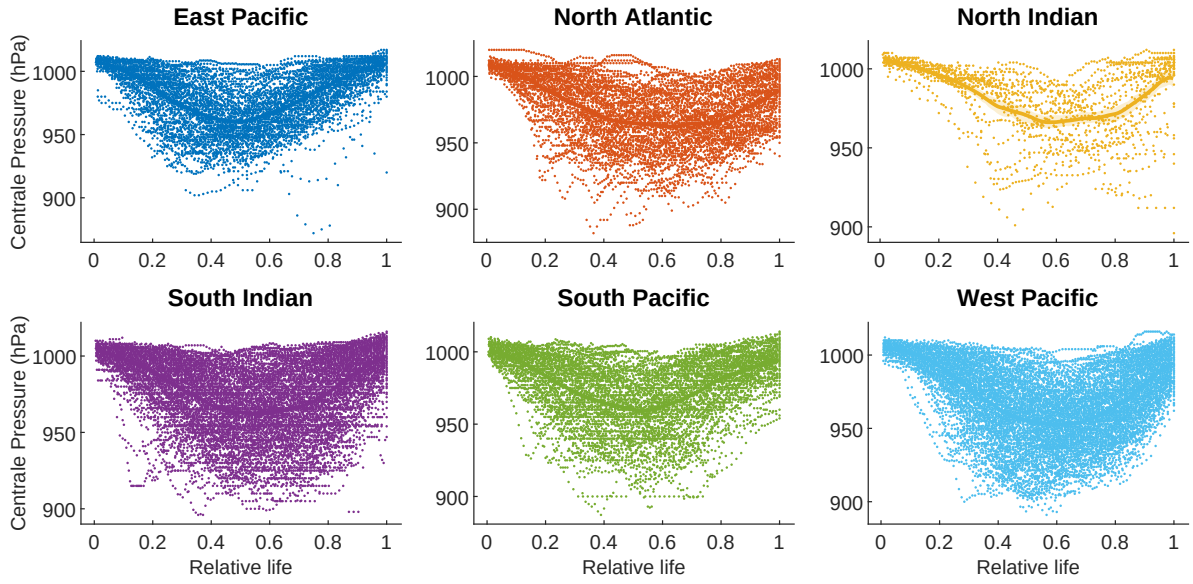

Figure 2. Normalized evolution of the central pressure (in hPa) during ~~cyclone~~ cyclones life~~of a sample of 100 storms for each basin~~. The ~~dotted line represents the average pressure evolution. The~~ central pressure values are retrieved from IBTrACS. For the West Pacific we reduced the sample to events between 1995 and 2020 for visualisation purpose.

~~Central pressure and maximum wind speed evolution for most damaging named cyclones in the North Atlantic (NA) basin. The values are retrieved from IBTrACS.~~

.[6]

$$A_{pix} = A_{tot} \frac{L_i \cdot P_{pix}}{\sum_{pix_i}^{N} (L_i \cdot P_{pix_i})}. \quad (1)$$

The physical asset value is expressed in USD as of 2014. Using this dataset in the future ~~might require~~ requires correcting (either simulated or reported damages) by inflation using~~for instance~~ , for instance, the consumer price index[7].[7]

170 This method for allocation of national assets has limitations. For example, the distribution of assets near the coast, industrial production sites or agricultural facilities may not be well represented. However, with this approach asset values are defined on a uniform grid across countries and can be projected by multiplication with appropriate dynamic factors.

[6] The values of A_{pix} on a 30 arc-second grid are available at https://www.research-collection.ethz.ch/handle/20.500.11850/331316.

[7] ~~Available at: .~~

[7] Available at: https://fred.stlouisfed.org.

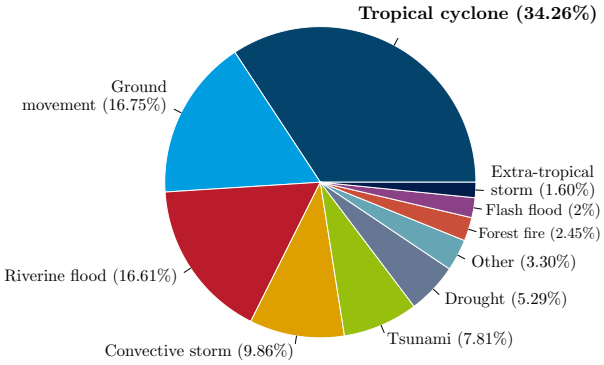

Figure 3. Proportion of damage cost (total damage in USD) by disaster subtypes reported in EM-DAT. Using the number of people affected places tropical cyclones after riverine floods and droughts, and the number of deaths places ground movements in first position (see Table A1 for details).

2.5 Global disaster database (EM-DAT)

The fitting of the damage functions was performed by Eberenz et al. (2021) on reported damages in the EM-DAT database (Guha-Sapir et al., 2018)[8]. Filtering the database by sub-type 'tropial cyclone' allows us to extract 1855 tropical cyclones in the period between 1980 and 2021, among which 1101 events have a reported total damage cost in USD (See Figure 4). In terms of damage, tropical cyclones are, using the full set of observations from 1980 to 2021, the most damaging events reported (see Figure 3). This database includes a start date field (day, month and year) allowing us to map ~~455 events~~455 events, with the events reported in IBTrACS using start year and month and country[9]. We use this database to validate our simplified estimation process.

2.6 The Shared Socioeconomic Pathways (SSPs) framework

Future exposure is sensitive to the scenarios of population growth and economic development. To take this into account, we use the framework of the shared socioeconomic pathways (SSP) introduced in O'Neill et al. (2014). These narratives are used in the IPCC development scenarios and provide a reference framework for risk assessment. A growing segment of the literature

[8] ~~available at :.~~
[8] Available at: www.emdat.be.
[9] ~~Eberenz et al. (2021) functions are fitted on a similar sample of 376 tropical cyclones used for calibration.~~
[9] Eberenz et al. (2021) functions are fitted on a similar sample of 376 tropical cyclones used for calibration.

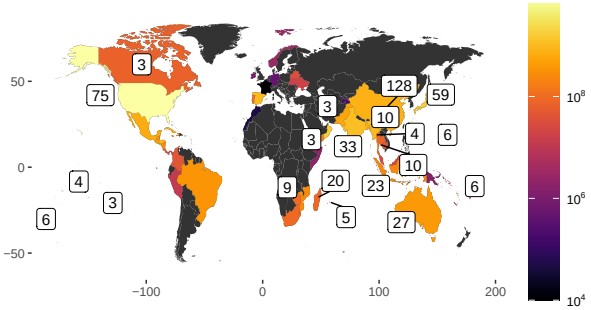

Figure 4. Number of tropical cyclones with reported damage cost in EM-DAT database. The color scale indicates the average reported damage cost in USD in each country for each tropical cyclone.

is dedicated to measuring the feasibility, costs and implications of achieving these scenarios (Riahi et al., 2017, 2021) and multiple Integrated Assessment Models (IAMs) were launched on assumptions based on these narratives (Riahi et al., 2017; Rogelj et al., 20 .[10] Figure 5 displays the projections of the main features used by CATHERINA, the global domestic production (GDP) and population in the five SSPs at the global level by the IIASA GDP model.[11] CATHERINA uses these two indicators at regional level (32 regions are available) to compute future local exposure (see section 4.5).

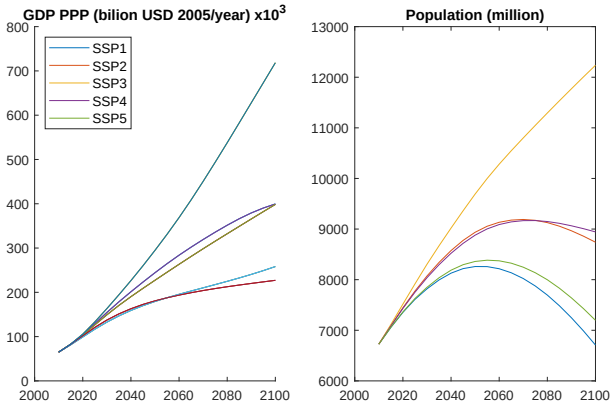

Figure 5. SSP GDP and Population variation until 2100, at global scale, by the IIASA GDP model

We reiterate the main features underlying these narratives. The '*middle road*' pathway (SSP2) is used as the reference in most scenario analyses. It is a plausible baseline in terms of economic and social resiliency, in which the urbanization level is relatively high and GDP and population are constantly increasing following the observed historical trend. On the other hand, the '*rocky road*' or '*national-rivalry*' pathway (SSP3) presents totally different properties: relative stagnation of GDP with a strong increase of the population (See Figure 5). SSP4 corresponds to a scenario with the highest inequality and SSP5 is

[10] For example, for the variable of interest, the outputs of IIASA GDP, IIASA-WiC POP, NCAR, PIK GDP-32, OECD Env-Growth models are available.
[11] Variables relative to SSPs are available here: https://tntcat.iiasa.ac.at/SspDb/.

the most likely to lead to the higher concentration pathways (RCP8.5), with extensive use of fossil fuel reserves but higher economic development and global markets integration.

Based on these storylines, it is clear that the physical exposure to tropical cyclones will be driven by different factors in different SSP scenarios. Scenarios with steady growth of GDP are generally associated with an increase in urbanisation but a decrease in the global population by 2050. In general, all narratives, except the SSP3, present relatively similar population dynamics at the global level. On the other hand, the scenario with the lowest economic growth (SSP3) presents a sustained increase of the population (cf. Figure 5), in particular in rural areas. We can therefore expect, in the former case, the physical asset value exposure to be driven by the increase of regional wealth, and mainly by the growth of the exposed population in the latter.

In this paper, we specify economic and climate parameters independently while the literature generally associates specific SSP and RCP, in particular in the CMIP6 exercise. Indeed, integrated assessment modeling demonstrates that specific temperature targets can only be reached under some socioeconomic conditions. The socioeconomic and representative concentration pathways are therefore intrinsically linked at the global scale. For example, CMIP6 refers to the following scenarios: SSP1-1.9, SSP1-2.6, SSP2-4.5, SSP3-7.0, and SSP5-8.5. On the other hand, this pairing is not straightforward at the regional level. In particular, the SSP2 scenario is associated with regional heterogeneity in socioeconomic pathways. As a result, although we can expect a convergence in the long run, we considered it relevant to use economic development scenarios independently from RCP in this exercise.

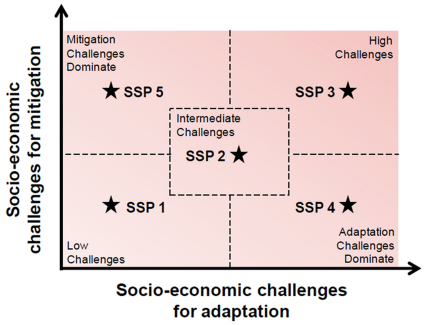

Figure 6. SSP Matrix (O'Neill et al., 2017)

Lastly, we acknowledge another limitation of our approach: The vulnerability parameter (represented by the damage function parameter v_b in our framework) does not depend on the SSP, while we could expect a reduction in the vulnerability parameter in the scenarios where the adaptation challenges are limited, such as SSP5 (cf. Figure 6). This question is left for further research.

3 Cyclone generation algorithm

Our model structure follows Bloemendaal et al. (2020) with three main modeling steps: genesis, displacement of the eye and calibration of the cyclone properties. The STORM model relies on statistical relationships (James and Mason, 2005; DeMaria and Kaplan, 1994; Kaplan and DeMaria, 1995). This simulation method differs from the purely thermodynamic approach developed by Kerry Emmanuel (Emanuel, 1999; Emanuel et al., 2008).

The major change in our specification compared to Bloemendaal et al. (2020) is that we use ~~a~~ the local definition of ~~maximum available thermodynamic intensity (MPI)~~ the available thermodynamic potential based on climate data. In particular, we use relative humidity (RH) and tropopause temperature (at 50 hPa, ~~T_{tropo}~~ T_{tropo}), for better theoretical representation of the physics underlying the intensification process. In this section, we present the process of generating synthetics tracks, characterized by the maximum wind (V_t) and central pressure (P_t^c) at each time step, given the climate conditions extracted from climate models.

3.1 Cyclone genesis

The scientific consensus is that climate change will induce a reduction in tropical cyclone frequency: "*Existing modeling studies also consistently project decreases in the globally averaged frequency of tropical cyclones, by 6 to 34%. Balanced against this, higher resolution modeling studies typically project substantial increases in the frequency of the most intense cyclones*" (Knutson et al., 2020, 1). Although thermodynamic descriptions of cyclone genesis exist in the literature (Gray, 1975; DeMaria et al., 2001) ~~, there is still too much uncertainty about how climate change will affect the frequency of cyclones to justify the integration of multiple additional variables at this step. For this reason,~~ we choose to rely on a simple statistical model based on past frequencies for the genesis.

The number of synthetic cyclones each year is determined by the Poisson distribution in each basin, with ~~parameter λ_B~~ intensity parameter defined as the average number of cyclones per year in the historical data. We use the parameters ~~λ_B~~ given in Bloemendaal et al. (2020) i.e. ~~14.5~~ $\hat{\lambda}_{\text{EP}} = 14.5$ for the East Pacific~~(EP), 10.8~~, $\hat{\lambda}_{\text{NA}} = 10.8$ for the North Atlantic~~(NA), 2.0~~, $\hat{\lambda}_{\text{NI}} = 2.0$ for the North Indian~~(NI), 12.3~~, $\hat{\lambda}_{\text{SI}} = 12.3$ for the South Indian~~(SI), 9.3~~, $\hat{\lambda}_{\text{SP}} = 9.3$ for the South Pacific~~(SP), and 22.5~~, and $\hat{\lambda}_{\text{WP}} = 22.5$ for the West Pacific~~(WP)~~[12]~~.~~. The parameters would have been smaller if estimated using our filtered database of tropical cyclones with wind speed above 35 m.s^{-1}: $\hat{\lambda}^{35}_{\text{EP}} = 7.31$, $\hat{\lambda}^{35}_{\text{NA}} = 4.43$, $\hat{\lambda}^{35}_{\text{NI}} = 1.6$, $\hat{\lambda}^{35}_{\text{SI}} = 6.81$, $\hat{\lambda}^{35}_{\text{SP}} = 4.00$ and $\hat{\lambda}^{35}_{\text{WP}} = 11.86$. However, we maintain the original parameters used in STORM to take into consideration the fact that some events will be generated in conditions not favorable for the development of cyclones and cleared out of the database. The number of cyclones making landfall being critical for damage estimation (Hall and Jewson, 2007; Lee et al., 2018; Arthur, 2021), we ensured that the simulated landfall rates are in line with the observations over the historical period: Figure 7 shows that the parameters of Bloemendaal et al. (2020) lead to approximately the same number of intense cyclones making landfall per year in each basin in the historical data, in our simulations based on reanalysis data and in simulations based on CGMs. We

[12] ~~The parameters λ_B would have been smaller if estimated using our filtered database. However, we maintain these parameters to take into consideration the fact that some events will be generated in conditions not favorable for the development of cyclones, and be cleared out of the database.~~

note however that the framework can be further improved by choosing the intensity parameter to match exactly the average historical number of cyclones making landfall.

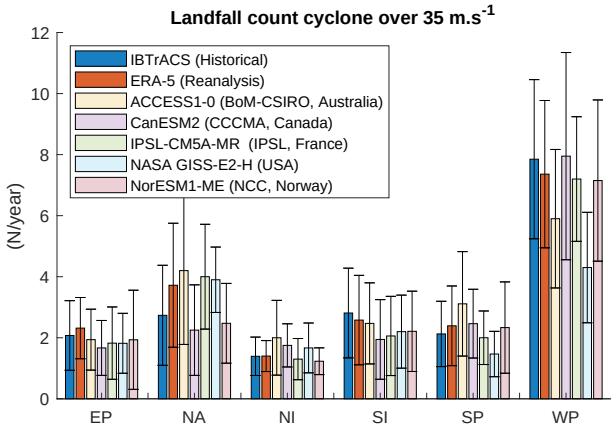

Figure 7. Number of tropical cyclones over 35$\mathrm{m.s}^{-1}$ making landfall simulated using Bloemendaal et al. (2020) parameters over the historical period (1980-2010)

Similarly, the temporal and spatial initial positions of synthetic future cyclones (longitude x, latitude y and starting month m) are generated by independent sampling from the historical distribution of these variables. Figure 8 shows the geographical distribution of cyclones retrieved from IBTrACS (i.e. x_{obs}, y_{obs}) and the histograms in Figure 9 show the monthly distribution (m_{obs}) of cyclones in each basin.

3.2 Cyclone trajectories

A rich literature focuses on cyclone tracking algorithms, see e.g., Neu et al. (2013) for a comprehensive review. Although more advanced definitions have been proposed (Hall and Jewson, 2007; Fabregat et al., 2016), we choose, in line with Bloemendaal et al. (2020), to implement a simple auto-regressive model for cyclone coordinates. Following James and Mason (2005), the time evolution of the latitude and longitude of the cyclone center is described by the following stochastic dynamics:

$$\Delta x_t = a_0 + a_1 \Delta x_{t-1} + \varepsilon_t^x, \qquad \varepsilon_t^x \sim \mathcal{N}(0, \sigma_x), \tag{2}$$

$$\Delta y_t = b_0 + b_1 \Delta y_{t-1} + \frac{b_2}{y_t} + \varepsilon_t^y, \qquad \varepsilon_t^y \sim \mathcal{N}(0, \sigma_y). \tag{3}$$

Here x_t and y_t are the latitude and longitude of the cyclone center sampled with a 3 hour time step; $\Delta x_t = x_t - x_{t-1}$, $\Delta y_t = y_t - y_{t-1}$, ε_t^x and ε_t^y are i.i.d. noises independent from one another, and the constants a_0, a_1, b_0, b_1, b_2, σ_x and σ_y are fitted on IBTrACS data independently for each basin by least squares regression. ~~Their values are provided in the Appendix. The nonlinear~~ The non-linear term in the incremental variation of the latitude is justified by the tendency for cyclones to move away from the equator, especially at very low latitudes (James and Mason, 2005, p. 183).

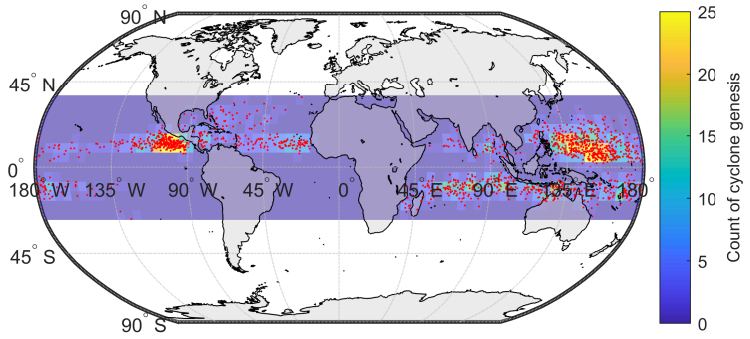

Figure 8. Spatial distribution of genesis points (~~all~~ tropical cyclones over 35$\mathrm{m.s}^{-1}$ in IBTrACS). ~~Made with Natural Earth~~The color scale corresponds to the count of cyclone per 5x5° box (truncated to 25 for scaling reason). The genesis location corresponds to the first reported point of each track.

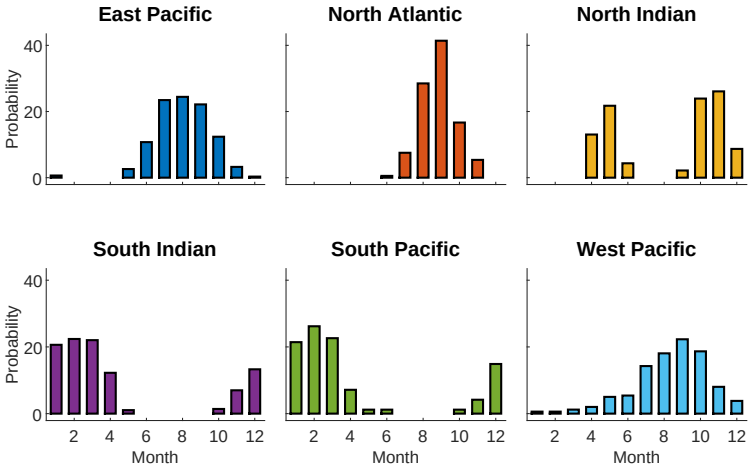

Figure 9. Relative monthly distribution (%) of cyclones in each basin defined from potentially damaging cyclones ~~filtration~~ (over 35$\mathrm{m.s}^{-1}$) in IBTrACS. Each bar gives the probability for each cyclone to be allocated to a given month.

~~We found this formulation sufficient for global assessment despite its lack of consideration for dependencies in the latitudinal and longitudinal variations (James and Mason, 2006)~~[12]~~. A sample of~~ To take into account the dependency of the ~~resulting tracks is provided in Figure ??~~cyclone displacement on the location of the eye, and following Bloemendaal et al. (2020), we fitted these relationships locally using an additional grouping by 5° longitude and latitude sections and months. Figure A2 illustrates the parameters a_0 and a_1, the adjusted R^2 and the number of observation averaged over months used to fit the Equation (2).

[12] ~~To reduce this effect and better encompass the dependency of the cyclone displacement on the location of the eye, and following Bloemendaal et al. (2020), we fitted these relationships locally using an additional grouping by 5longitude and latitude sections.~~

We note that the trajectories in North Indian basin are less well captured in some areas, particularly longitudinal movements near the coast from Yemen, Oman and the United Arab Emirates (see maps of adjusted R^2 in Figure A2).

~~Synthetic tracks generated with ERA-5 climate data for the period 1980-2010. Made with Natural Earth.~~ This statistical definition of cyclone trajectories does not consider changes in track behaviour. For example, observed trends in tropical cyclone translation speed Kossin (2018) and poleward migration of maximum intensity Kossin et al. (2014) could be considered to improve the projections of tropical activity. This indeed has potential implications for tropical cyclone-related risk in some areas where vulnerabilities are high and the present-day frequency of tropical cyclones is low Bruyère et al. (2019).

3.3 Thermodynamic description of cyclone intensity

The intensity of cyclones in our model is defined through the following five steps described in ~~the~~ detail in subsequent paragraphs. The wind-pressure relationship (WPR) links the central pressure to the maximum 10 minute-sustained wind speed. The local thermodynamic maximum potential intensity (MPI) is determined from local meteorological variables. The maximum pressure drop (MPD) is determined from historically observed pressures. The depression dynamics (DD) along tracks is defined using an autoregressive stochastic equation. When the cyclone arrives on land, a statistical decay relationship (SDR) dictates the evolution.

3.3.1 Wind-pressure ~~relationship~~ relationships (WPR)

We describe the cyclone intensity through its central pressure P_t^c, which is linked with the maximum wind through an empirical relationship. Let V_t be the maximum 10-min sustained wind speed (in $\mathrm{m.s}^{-1}$)[12] of the cyclone at time t. This maximum wind is observed around 50 km away from the storm center on average[13] and reported in the IBTrACS dataset for historically observed cyclones.

The wind-pressure relationship (WPR) is calibrated ~~on the whole cyclone database as follows~~separately for each basin and takes the following form:

$$V_t = a\left(P_{env}(x_t, y_t, t) - P_t^c\right)^b, \tag{4}$$

where $P_{env}(x, y, t)$ is the mean ~~sea level~~ sea-level pressure (MSLP) extracted 500 km away from the eye location at this time in ERA-5 and P_t^c is the central pressure extracted from IBTrACS. This relationship is illustrated in Figure 10 and the parameters a and b are fitted on ERA-5 and IBTrACS data using nonlinear least squares.

We acknowledge that most cyclone track data use wind-pressure relations (WPRs) to determine P_c. The conversion back to wind speed from reported P_c using a basin-specific WPR still introduces errors, as different WPRs are used to operationally estimate P_c within each basin (Harper, 2002; Courtney, 2009; Courtney and Burton, 2018; Courtney et al., 2021). However,

[12] For the data from the World Meteorological Organisation (WMO) and the agencies reporting 1 or 3-minutes sustained wind speed, we performed the conversion to ~~10 minutes~~ 10-minutes sustained wind speed using the coefficients suggested by Knapp et al. (2010). See Figure A1 in the Appendix for more details about the agencies and reporting bias.

[13] Radii of maximum wind are also reported in IBTrACS but this information is not central for national level assessment.

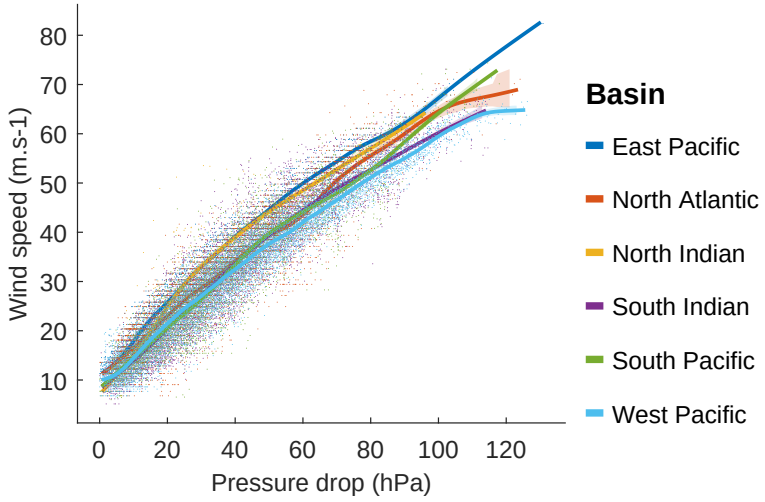

Figure 10. Maximum wind and pressure drop values from IBTrACS together with the fit of Equation (4). The ~~parameters, $a \sim 3.8$~~ coefficients a and ~~$b \sim 0.6$, depend slightly on the method for filtering the cyclones~~b fitted per basin are provided in Table **??**.

given the similarity of the relationships, we find that basin-level estimations are a sufficient proxy in the context of this illustration of the CATHERINA framework.

3.3.2 Local thermodynamic maximum potential intensity (MPI)

We compute the local thermodynamic maximum potential intensity (MPI) following ~~Holland (1997) and using thermodynamic relationships .~~ the thermodynamic relationships defined in Holland (1997). This is particularly relevant in the context of a national damage assessment under a changing climate. ~~Indeed, greenhouse~~ Greenhouse gas emissions not only warm up the oceans ~~,~~ but also cool down the lower stratosphere (Butchart et al., 2000; Forster et al., 2007; Ramaswamy et al., 2006). Thus, the tropopause temperature ~~T_{tropo} (~~ - that is, the temperature corresponding to a pressure of 50 hPa or to an altitude of approximately 20 km ~~))~~ available in multi-level CMIP dataset (T_{tropo}) must be included in the modeling of the intensification process. Indeed, the thermodynamic efficiency factor ~~$\mathcal{E}_t$~~ $\mathcal{E}_t$ proportional to the difference between tropopause and ~~sea surface~~ sea-surface temperatures plays an essential role in the determination of the central pressure of tropical ~~cyclone~~cyclones. The relative humidity (RH) (which changes with climate change, see Sherwood et al. (2010)) is also an influential parameter allowing for a better description of ~~MPI~~[14] thermodynamic potential enabling cyclone intensification. Adding these two climate variables ~~allows~~ enables the CATHERINA model to better take into account the additional energy potential due to the widening of temperature ~~difference between sea surface~~ differences between the sea-surface and upper troposphere and variation in moist entropy.

[14] ~~In addition this parameter changes with climate change (Sherwood et al., 2010).~~

Following the seminal formulation in Emanuel (1988) and integrating additional simplifications proposed in the subsequent paper (Emanuel, 1991)~~to simplify the expression~~, leads to the following framework summarized in Holland (1997).

$$\mathrm{MPI}_t = \mathrm{MSLP}(x_t, y_t, t) \cdot \exp^{-X_t}, \tag{5}$$

$$X_t = \frac{\mathcal{E}_t \cdot \mathrm{SST}(x_t, y_t, t) \cdot \Delta S_t^m - \frac{f(y_t)^2 r_{env}^2}{4}}{R_d \cdot \mathrm{SST}(x_t, y_t, t)}, \tag{6}$$

$$\mathcal{E}_t = \frac{\mathrm{SST}(x_t, y_t, t) - T_{\mathrm{tropo}}(x_t, y_t, t)}{\mathrm{SST}(x_t, y_t, t)}, \tag{7}$$

$$\Delta S_t^m = R_d \ln\left(\frac{\mathrm{MSLP}(x_t, y_t, t)}{P_{t-1}^c}\right) + \frac{L_v(q_{ct}^\star - q_t^{env})}{\mathrm{SST}(x_t, y_t, t)}, \tag{8}$$

$$q_{ct}^\star = \frac{3.08}{P_{t-1}^c} \frac{3.08}{P_{t-1}^c} \exp\left(\frac{(\mathrm{SST}(x_t, y_t, t) - 273.15)}{\mathrm{SST}(x_t, y_t, t) - 29.65}\right), \tag{9}$$

$$q_t^{env} = \frac{3.08 \cdot \mathrm{RH}(x_t, y_t, t)}{\mathrm{MSLP}(x_t, y_t, t)} \times \exp\left(\frac{17.67\,(\mathrm{SST}(x_t, y_t, t) - 273.15)}{\mathrm{SST}(x_t, y_t, t) - 29.65}\right). \tag{10}$$

where (x_t, y_t, t) are the coordinates of the eye defined in Equations (2) and (3), ~~$\mathrm{SST}(x_t, y_t, t)$~~ $\mathrm{SST}(x_t, y_t, t)$ and $T_{\mathrm{tropo}}(x_t, y_t, t)$ are respectively the sea-surface and tropopause temperatures, $R_d = 287.058\ \mathrm{J \cdot kg^{-1} \cdot K^{-1}}$ is the specific gas constant for dry air, $\mathrm{MSLP}(x_t, y_t, t)$ is the mean local ~~sea level~~ sea-level pressure, $\mathrm{RH}(x_t, y_t, t)$ is the near surface relative humidity at 2 meters extracted from the monthly dataset of ERA-5 climate reanalysis or CMIP climate models. $f(y_t) = 2\omega \sin(y_t)$ is a Coriolis parameter depending on the latitude, r_{env} is the distance between the eye and the area under regular conditions (fixed at 500 km), q_{env} and q_c^* respectively are the specific humidity at environmental conditions and at saturation, i.e. for $\mathrm{RH} = 100\%$, in the eye. ΔS^m is the difference of moist entropy between the environment and the storm center and L_v is the latent heat of vaporization. The distributions of the ~~variables~~ climate variables and the instrumental indicators computed from ERA-5 climate variables along IBTrACS involved in this step are shown in Figure 11. ~~The distance to MPI is computed as the difference between the central pressure and the maximum potential intensity (MPI) defined in Equation (5).~~

3.3.3 Maximum pressure drop (MPD)

Several papers, including Bloemendaal et al. (2020), link the ~~sea surface~~ sea-surface temperature directly to the pressure drop, or equivalently the wind speed, via a statistical relationship (DeMaria and Kaplan, 1994). Merrill (1987) suggests that this predictor alone does not provide a good indication of whether a given storm will intensify. However, in line with Emanuel (1988) and DeMaria and Kaplan (1994) the ~~sea surface~~ sea-surface temperature can be used to fix a limit for the pressure drop. ~~More precisely~~Thus in CATHERINA, to prevent the pressure drop from diverging in the projection, we cap it by the maximum observed pressure drop for the corresponding ~~sea surface~~ sea-surface temperature:

$$P_t^c := \max(P_t^c, \mathrm{MSLP}(x_t, y_t, t) - \mathrm{MPD}(\mathrm{SST}(x_t, y_t, t))),$$

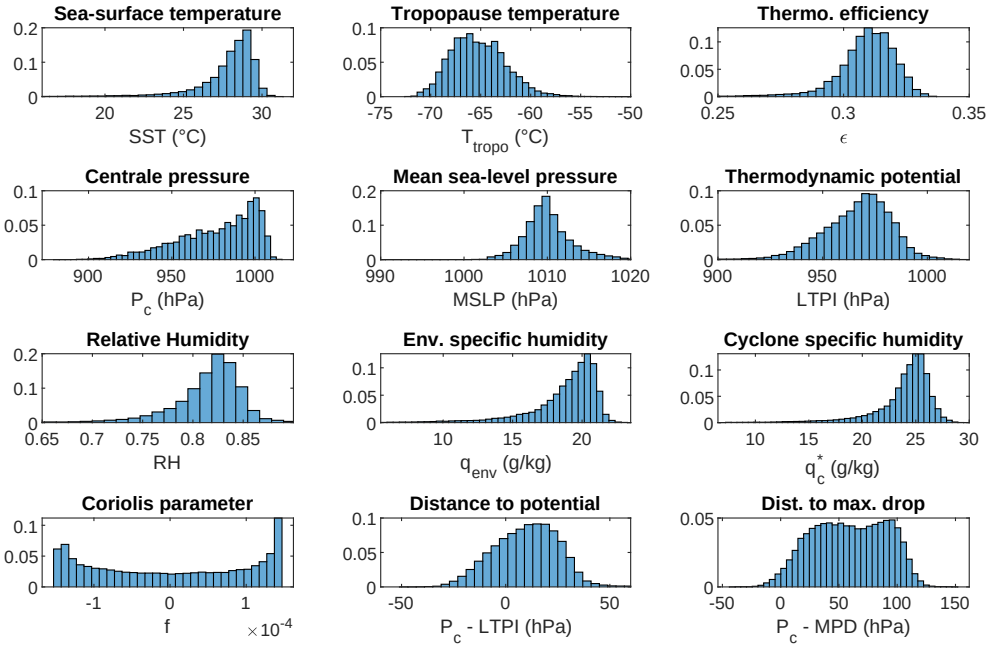

Figure 11. Empirical distribution of physical properties along tracks (IBTrACS and ERA-5), and distribution of instrumental variables of CATHERINA

where the maximum pressure drop function is given by the following equation:

$$\mathrm{MPD}(\mathrm{SST}) = A + B \cdot e^{C(\mathrm{SST}(x_t, y_t, t) - T_0)} \tag{11}$$

with T_0 = ~~30.0~~30°C. To fit this functional relationship, we first retrieve, for each basin, and for each value of the ~~sea surface~~ sea-surface temperature SST, rounded at 0.1, the maximum observed value of the pressure drop in the basin. These values are shown as crosses in Figure 12. The coefficients A, B and C from relationship (11) are then fitted to these values by nonlinear least squares. The resulting MPD functions for each basin are shown in Figure 12 as solid lines.

The definition of the MPD is identical in STORM and CATHERINA, but the role of this quantity differs in the two models. Figure 12 gives a ~~somewhat~~ misleading idea about the strength of correlation between the ~~sea surface~~ sea-surface temperature and the central pressure: indeed, fitting the distribution on the full sample (instead of just the maximum pressure drop for each temperature value) shows a much weaker influence of ~~sea surface~~ sea-surface temperature alone, even on a weekly basis (see Jien et al. (2017)~~and Figure ?? in the Appendix).~~). However, this instrumental variable is essential to prevent CATHERINA from producing unrealistically low central pressure. On the other hand, limiting the maximum pressure drop in simulations to the parametric function given by equation (11) fitted by non-linear least squares to the observed MPD leads to an excessively strong limitation on the intensity of the simulated cyclones, since many points in Figure 12 (lower graph) are above the red curve. Therefore, we shift this parametric function upward to the highest observed point to relax this limitation.

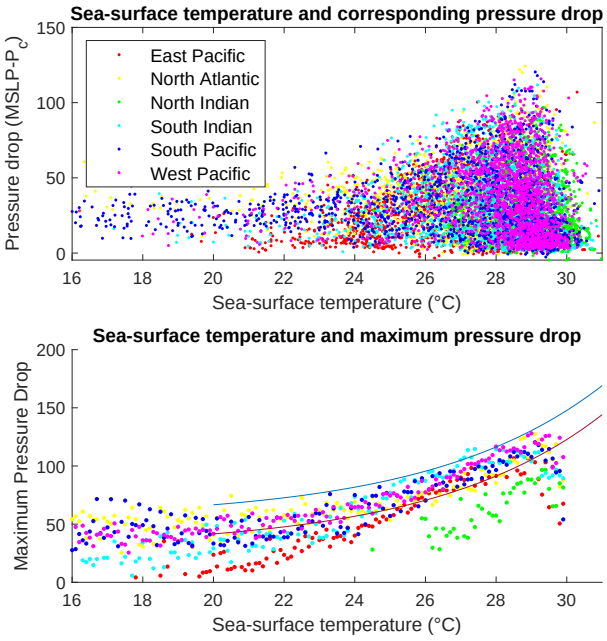

Figure 12. ~~Maximum~~ Top: full distribution of observed pressure drop values for given SST~~(crosses) and the fit of equation Equation (11)~~ . Bottom: maximum observed pressure drop values for ~~each basin (solid lines)~~given SST. The ~~dotted~~ red line shows the ~~calibration~~ least squares fit of Equation (11)~~simultaneously~~ , which corresponds to ~~all basins (~~parameter values $A = 30.6$, $B = 86.3$ and $C = 0.19$~~)~~. The blue curve is the capping function used to prevent unrealistic pressure drops, obtained by shifting the red curve upwards.

3.3.4 Depression dynamics (DD)

The evolution of the central pressure depending on ~~local MPI is~~ the intensification factor Y_t (which is defined differently in our approach and in STORM, as we explain below) is described by the following autoregressive stochastic ~~depression dynamics (James and Mason, 2005):~~ equation (James and Mason, 2005):

$$\Delta P_t^c = c_0 + c_1 \Delta P_{t-1}^c + c_2 e^{-c_3[P_t^c - \mathrm{MPI}_t] - c_3[P_t^c - Y_t]} + \varepsilon_t^P, \tag{12}$$

$$\varepsilon_t^P \sim \mathcal{N}(0, \sigma_{P^c}), \tag{13}$$

~~where the distance to maximum potential , $P_t^c - \mathrm{MPI}_t$, enters as a non-linear term in the dynamic definition~~ This relationship channels the effect of global warming, affecting the thermodynamic potential constructed with climate projections, on the cyclone intensity. Thus, the incremental variation of the central ~~pressure "*providing an increasing tendency for Δp to be positive as the central pressure approaches the mean MPI for the cyclone's location*" (James and Mason, 2005, p. 183). The parameters are fitted on historical tracks using ERA-5 reanalysis with nonlinear least squares (see Table **??**) . The confidence intervals show non-negligible variations, however, the coefficients remain statistically significant and of the expected sign. This~~

~~relationship channels the effect of global warming, affecting the maximum potential~~ depression of the cyclone is linked to the difference between the central pressure at time t and the potential available in the environment.

The intensification module of CATHERINA is inspired by STORM (Bloemendaal et al., 2020). The main differences are the definition of the thermodynamic maximum potential intensity (MPI) used in Equation (12) and the role of played by the maximum pressure drop (MPD). In Bloemendaal et al. (2020), the MPI is defined subtracting the maximum pressure drop (MPD) from the normal environmental pressure (MSLP) where the MPD is defined as a function of the SST and Bister and Emanuel (2002) values are used to bound their values. On the other hand, we define the thermodynamic intensification factor following Holland (1997) with variables extracted along the synthetic tracks and use the SST-MPD relationship as a capping function (see Figure 12). Table **??** summarizes the main differences of the two approaches.

As illustrated in Figure 13, both methods produce a similar dependence of the intensitication function (12) on the distance to potential and maximum pressure drop. When P_c approaches the local maximum potential intensity (or maximum pressure drop), ΔP^c is more likely to be positive and to decrease the storm intensity~~, on the cyclone intensity~~. In other words, ~~the incremental variation of the central depression of the cyclone is linked tothe difference between the central pressure at time t and the potential available in the environment.~~ we can distinguish two phases (see Figure 13, left graph): the intensification phase (in blue), when the central pressure is above the local MPI threshold, and a decay phase (in red) where the central pressure is below this local MPI.

In contrast to the MPD, the MPI does not represent the maximum achievable pressure and can be exceeded when accounting for additional external factors not reflected in climate data. For example, Chen et al. (2021) suggest that rapid intensification also depends on dynamical factors (e.g. upper divergence and wind shear). While James and Mason (2005) formulation implicitly assumes that these factors are accounted for in the residual term of Equation (13), it does not consider that the distance to the maximum potential thus defined, can take negative values. Indeed, this specification originally suggests using the maximum achievable central pressure, therefore that $P_c - \mathrm{MPI} > 0$. As a result, the two intensification factors are not defined on the same domain (see Figure 11). Using the local thermodynamic MPI, negative values, corresponding to a situation where the central pressure is below the MPI ($P_c < \mathrm{MPI}$), are associated with a positive response of the pressure dynamic module, and an decrease in storm intensity. Using the MPD, the response (is likely to) become positive when distance to MPD is below 40 to 60 hPa, depending on whether the function has been applied to the local sea-surface temperature or the maximum per grid box ($5° \times 5° \times$month). Given the similar response provided, using the local MPI instead of MPD as the intensification factor offers a better theoretical representation of the conditions affecting cyclone intensification in the cyclone dynamic module. The central pressure dynamics used for the fitting and the dynamics of the synthetic tracks produced in the north Atlantic basin are illustrated in Figure 14. The intensification of synthetic cyclones is in line with historical observations.

3.3.5 Statistical decay relationship (SDR) over land

We model the evolution of the cyclone after landfall using an exponential decay function considering that ~~"*tropical cyclone intensity decreases as a function of the time and distance the tropical cyclone has covered whilst being over land*"~~ tropical cyclone intensity decreases as a function of the time and distance the tropical cyclone has covered whilst being over land

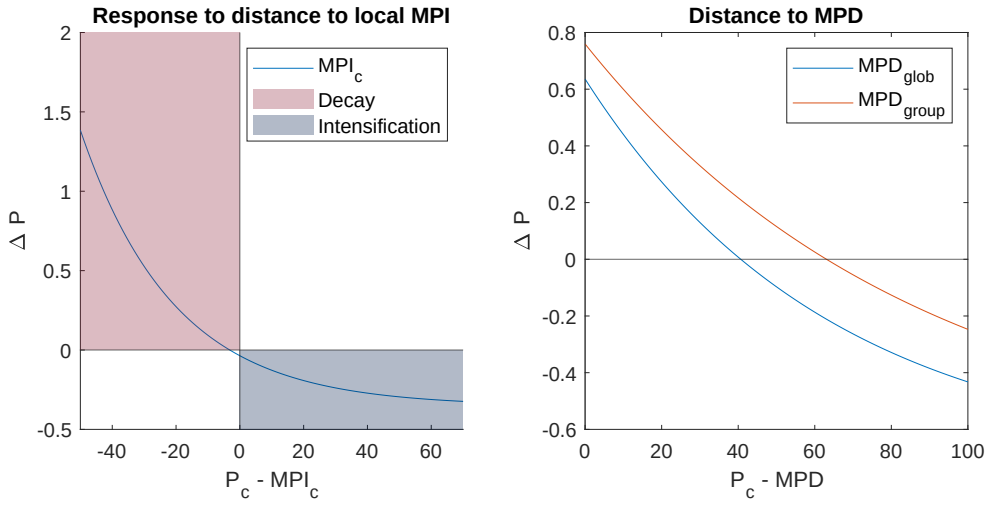

Figure 13. ~~James and Mason (2005) depression dynamics (Equation 12) parameters , standard errors and confidence intervals estimated using nonlinear least squares on~~ Response of the ~~full sample. The MPI is computed based on the climate data extracted along tracks from ERA-5, and the~~ depression dynamics ~~are derived from IBTrACS~~ model to distance to thermodynamic potentials over intensification factor domains

~~EstimateStd. Error2.5% 97.5%c_0 17.966 3.161811.77024.162c_1 -0.516 0.00274-0.522-0.510c_2 -19.528 3.180 -25.760-13.295c_3 0.00776 0.00134 0.0050.010~~

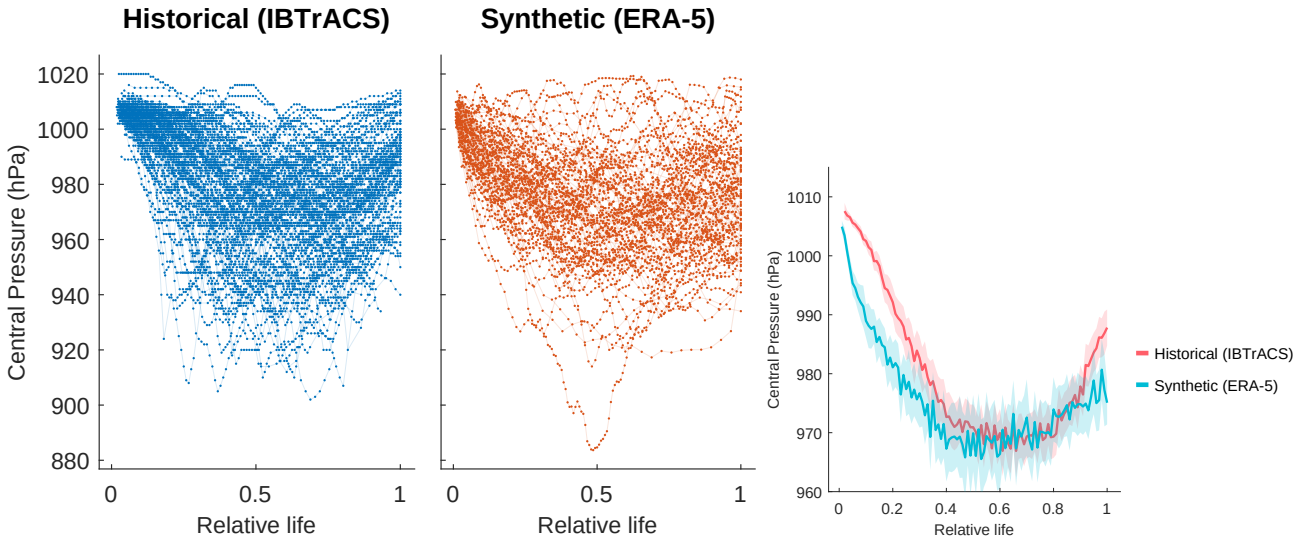

Figure 14. ~~Depression and wind evolution over cyclones lifetime (top winds in synthetic tracks)~~Individual historical vs. ~~We observe similar~~ Synthetic depression dynamics ~~as~~ in ~~Figures 2~~ North Atlantic Basin, and ~~??~~confidence interval.

(Kaplan and DeMaria, 1995). Similarly to Bloemendaal et al. (2020), after three steps on land we suppose that the wind at time t_L follows:

$$V_{t_L} = V_b + (R \cdot V_0 - V_b)e^{-\alpha t_L} - f_1(t_L)\left(\ln \frac{D^l}{D_0}\right) + f_2(t_L) \quad (14)$$
$$= V(t_L, D^l, V_0).$$

where D^l is the distance to coast computed using natural earth coastlines[14], [14] V_0 is the wind at landfall and t_L the time spent on land by the eye. This function was fitted on IBTrACS using nonlinear least squares. In our procedure, we use the global [15] parameters: $R = 0.79$, $V_b = 15\ \mathrm{m.s^{-1}}$, $\alpha = 0.044\ \mathrm{h^{-1}}$, and $f_1(t_L) = \tilde{c}_1 t_L(t_{0,L} - t_L)$, $\tilde{c}_1 = 3.35.10^{-4}\ \mathrm{ms^{-1}h^{-2}}$, $t_{0,L} = 172\ \mathrm{h}$, $f_2(t_L) = d_1 t_L(t_{0,L} - t_L)$, $d_1 = -0.00186\ \mathrm{ms^{-1}h^{-2}}$ and $D_0 = 1\ \mathrm{km}$. Kaplan and DeMaria (1995) introduced this function to model the decay of tropical ~~cyclone~~ cyclones over land in a simple way and showed that it provides an acceptable approximation for ~~$t_L \geqslant 12h.$~~ $t_L \geqslant 12$ h. As each time step is 3 hours, we let the TC intensity be driven by Eq. (12) the first three steps and apply the decay function after three steps, that is, for $t_L \geqslant 12$ h. A more sophisticated description could integrate for instance, cyclone physics, kinetic energy, and non-meteorological parameters such as ground topology. The SDR puts a strong constraint on the cyclone evolution after three steps. However, in the context of national damage assessment we reiterate that reported damage costs are the combination of a series of various impacts including storm surge and not only extreme wind and that the most exposed area is at landfall. We consider therefore that the hypothesis of a rapid decay is acceptable and in line with observations.

3.4 Cyclone generation algorithm

The full cyclone generation procedure is presented in Algorithm 1. The cyclone wind speed is initiated at 20 $\mathrm{m.s^{-1}}$ and the initial pressure is determined from the WPR (Equation (4)). While the cyclone is over sea, the pressure evolution ΔP_c is entirely determined from Equation (12) based on the local ~~MPI~~thermodynamic potential. To prevent the model from producing unrealistically low central pressure, we cap the maximum pressure drop (MPD) using Equation (11). With this truncation the lower bound for the pressure is given by the observed low pressure values in similar sea-surface temperature conditions. While the cyclone is over sea, the wind is defined with the WPR (Equation (4)). When the cyclone arrives on land the MPI is computed from the last known climate variables for the first three steps and the pressure still follows the relationship (12). After three steps (9h) on land, we start applying the decay relationship (Equation (14)) to define the wind. The variations of longitude and latitude are always defined using Equation (2) and Equation (3). We force cyclones to remain in their genesis basins in this exercise. For example, running the algorithm on IPSL climate projections between 2075 and 2100, in the RCP85 produces the output plotted in Figure 15.

The cyclone intensification process used is inspired by STORM model form Bloemendaal et al. (2020), which includes a single climate variable, and extended following Holland (1997) and Emanuel (1988) to encompass 2 more variables. We found

[14] ~~Available at .~~

[14] Available at https://www.naturalearthdata.com/downloads/10m-physical-vectors/.

[15] ~~The statistical parameters are stable and fitting this relationships with non-linear least square for each basin gives the parameters in Table ?? on page ??.~~

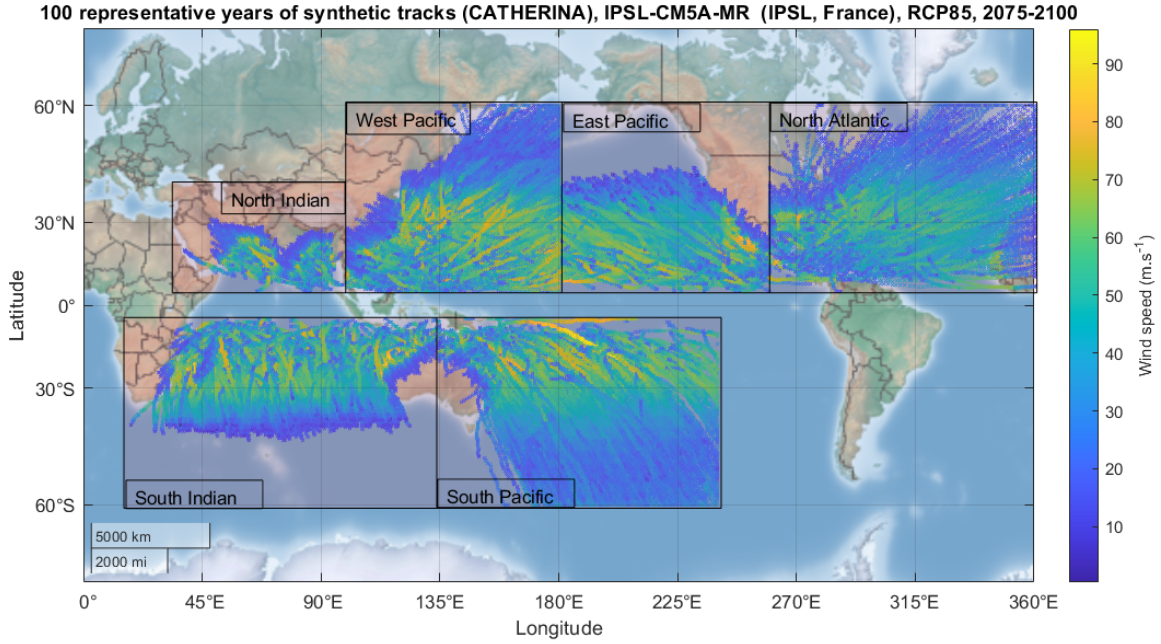

Figure 15. Example of 100 representative years of synthetic tracks produced with CATHERINA on IPSL-CM5A-MR raw climate data in the RCP85 between 2075-2100 (i.e. four runs over the 25 years period)

that this extension provides statistically significant instrumental variables in the description of tropical cyclone intensification, which is the aim of the algorithm. Consequently, even if some thermodynamic processes have been simplified in our approach, it is still a step forward with respect to the existing state-of-the-art in the field of integrated assessment modeling for climate impact analysis. Indeed, our approach is easy to implement, more sophisticated in terms of processes included than most existing IAM, has low bias due to our state of the art bias correction module described below, and can integrate any CMIP simulation with a limited set of available variables (only a few vertical levels, some only available at monthly time scale, with some variables not always available).

4 Damage assessment at the national level

4.1 Damage modeling

The percentage of asset value destroyed by a tropical cyclone depends ~~of~~ on multiple parameters. For example, to assess the vulnerability of specific infrastructures to tropical cyclones, precise descriptions of building vulnerability are provided in the Federal Emergency Management Agency (FEMA) reports. Unanwa et al. (2000) propose a series of ~~wind damage~~ wind-damage bands depending on building types. ~~For~~ The sensitivity is higher for commercial and institutional buildings ~~the sensitivity is higher~~ than for residential and mid-rise buildings. Unanwa et al. (2000) reveals that generalized damages occur above 43-60

$\mathrm{m.s^{-1}}$. ~~Sustained~~ A sustained wind regime above 73 $\mathrm{m.s^{-1}}$ could lead to the destruction of the entire superstructure of most buildings (expect for ~~mid~~ mid- and low-rise ones). Damages provoked by winds between 60 and 81 $\mathrm{m.s^{-1}}$ strongly depend on building components and connections. These bottom-up approaches allow us to set the limits of the potential damage functions, but their use requires a complete inventory of assets and up-to-date values of numerous parameters (age, height, materials, etc.). Therefore, CATHERINA relies on regional damage functions calibrated by Eberenz et al. (2021) on wind speed along cyclone track (IBTrACS) and reported damages in Guha-Sapir et al. (2018).

Damages provoked by tropical cyclones can be related to several sub-perils. While 40% of cyclone damages are directly wind-related, another 40% can generally be attributed to storm surge, and the rest of the damage is generated by heavy precipitation. However, CATHERINA does not distinguish these sub-perils, associated with key thermodynamical processes of cyclones (heavy precipitation, storm surge and associated flooding, strong winds) but uses a statistical relationship to estimate the regional global damage induced by a cyclone from a proxy variable given by the maximum wind speed. Indeed, the wind speed is the proxy used in the Saffir-Simpson Hurricane wind scale to define the intensity of a cyclone. The damage function is fitted on multiple events from the total damage reported in the global disaster database EM-DAT (Guha-Sapir et al., 2018) . This database, used in most studies on the topic, accounts for the total reported damage (sum of all sub-perils) and does not distinguish damages from sub-perils.

4.2 From an explicit damage function...

Damage functions can take several different forms (Prahl et al., 2015) but the most common choice is a cubic functional of the wind speed. To estimate the fraction of loss from a storm with sustained wind speed V, Emanuel (2011) introduced the following formula:

$$f(V, v_h^j) = \frac{\left(\max(V - v_0, 0)\right)^3}{(v_h^j - v_0)^3 + \left(\max(V - v_0, 0)\right)^3}, \tag{15}$$

where f is the fraction of the property value lost, $v_0 = 25.7\ \mathrm{m.s^{-1}}$ and v_h^j a parameter that needs to be calibrated for each region j. Figure 16 illustrates the shape of the damage function for different values of this parameter.

To account for adaptation we could modify this function and introduce an additional threshold value. For instance, to account for local adaptation to the wind climate, Leckebusch et al. (2007) suggest to scale the wind value by the 98th percentile of the local wind speed distribution. However, the assumption that adaptation will always keep the damages from the 98-percentile wind at the same level is probably optimistic, and will prevent us from using the model to estimate the required investment to balance future damages and economic shocks.

4.3 ... to a regional damage calibration

Using the reported damage estimates from the International Disaster Database (EM-DAT) crossed with cyclone tracks (IBTrACS), and geographical and socio-economic information along these tracks, Lüthi (2019) refined the damage function approach using machine learning techniques introducing region-specific damage functions.

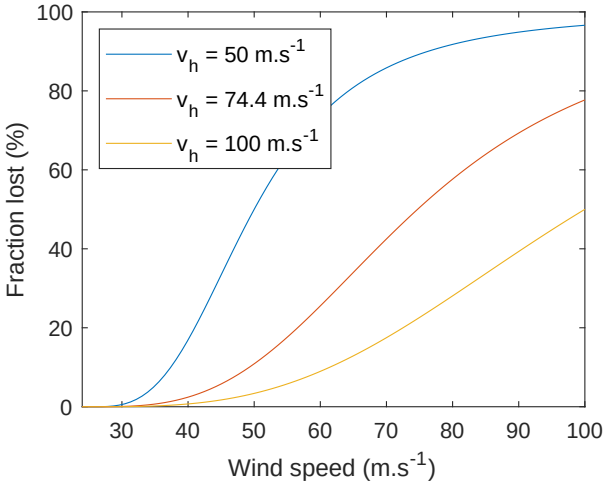

Figure 16. Fraction of property value lost as a function of wind speed, obtained using Equation (15) with ~~v_h^j = 50 (red), 74.4 (dark blue) and 100 (light blue)~~different values of v_h. Source: Emanuel (2011).

We recall the main steps of the methodology presented in ~~(Lüthi, 2019; Eberenz et al., 2021)~~ Eberenz et al. (2021) to define the regional damage functions. The authors first defined the event damage ratio (EDR) as a ratio of simulated damage (SED) to normalized reported damage (NRD) for each cyclone:

~~$$\mathrm{EDR}(i,j) = \frac{\mathrm{SED}(i, v_h(j))}{\mathrm{NRD}(i)}.$$~~

$$\mathrm{EDR}(i,j) = \frac{\mathrm{SED}(i, v_h(j))}{\mathrm{NRD}(i)}. \quad (16)$$

The total damage ratio (TDR) is then defined in each region summing over events:

~~$$\mathrm{TDR}(j) = \frac{\sum_i \mathrm{SED}(i, v_h(j))}{\sum_i \mathrm{NRD}(i)}.$$~~

$$\mathrm{TDR}(j) = \frac{\sum_i \mathrm{SED}(i, v_h(j))}{\sum_i \mathrm{NRD}(i)}. \quad (17)$$

For each event, there is a value for v_h allowing to optimally calibrate the explicit damage function given in Equation (15). The relatively wide distribution of v_h for the same country shows that there is a large uncertainty in the relationship between the wind speed and the corresponding fraction of losses[15]~~.~~. Figure A4 shows the uncertainty in regional damage functions

[15] ~~In the Appendix, Figure A4 shows the uncertainty in regional damage functions depending on the optimization technique used and Figure A5 allows us to appreciate, for countries where more than 5 cyclones were reported, the spread of plausible damage functions.~~

Table 2. Values of v_h obtained using TDR and RMSF methods for each region from the CLIMADA environment

Region	$v_h^\star{}_{\mathrm{TDR}}$	$v_h^\star{}_{\mathrm{RMSF}}$
Caribbean and Mexico (NA1)	58.8	59.6
China Mainland (WP3)	101.5	80.2
USA and Canada (NA2)	80.5	86
North Indian (NI)	63.7	58.7
South East Asia (WP1)	60.7	56.7
North West Pacific (WP4)	169.6	135.6
Philippines (WP2)	167.5	84.7
Oceania (OC)	56.8	49.7
South Indian (SI)	48.5	46.8
Global (GLB)	98.9	73.4

Coefficient from version 1.5 of the CLIMADA environment. Figure A4 also illustrates the shapes of the functions for the different optimization problems (RMSF vs. TDR) and version (1.0 vs 1.5).

depending on the optimization technique used and Figure A5 allows us to appreciate, for countries where more than 5 cyclones were reported, the spread of plausible damage functions.

~~The authors~~ Eberenz et al. (2021) propose two alternative optimization methodologies to find the value of $v_h^\star$ maximizing the prediction quality of the regional damages: root mean square fraction (RMSF), minimizing the spread of the event damage ratios (EDR)~~; and~~ :

$$v_h^\star{}_{\mathrm{RMSF}}(j) = \mathrm{argmin}_j \exp\left(\sqrt{\frac{1}{N}\sum\left(\ln(\mathrm{EDR(i)})\right)^2}\right), \tag{18}$$

and total damage ratio (TDR), finding the value of $v_h^\star$, such that the ratio of total simulated damage – obtained summing over event damages – and total reported damage tends to 1.

$$v_h^\star{}_{\mathrm{TDR}}(j) = \mathrm{argmin}_j \left|\mathrm{TDR}(j) - 1\right| \tag{19}$$

The values of ~~v_h obtained~~ $v_h^\star$ obtained by Eberenz et al. (2021) with the two methods are given in Table 2. For most regions, the optimized curves are similar for the two optimization techniques, but the results diverge for the Philippines (WP2) and to a lesser ~~extend~~ extent for China Mainland (WP3) events. The case of the Philippines, for example, discussed in Eberenz et al. (2021), is explained by the large number of parameters involved in the damage estimation, and emphasizes two main limitations of the model: ~~first~~First, this framework lacks an explicit representation of sub-perils ~~which~~ that disrupt and damage several sectors and services~~, and second,~~ . Second, differences in exposure and vulnerability between urban and rural areas exposed to ~~TCs~~ tropical cyclones are likely to contribute to the large spread in EDR.

~~(a) Asset data (30 arc-sec) (b) Rasterized map (0.25x0.25) (c) Interpolation along~~

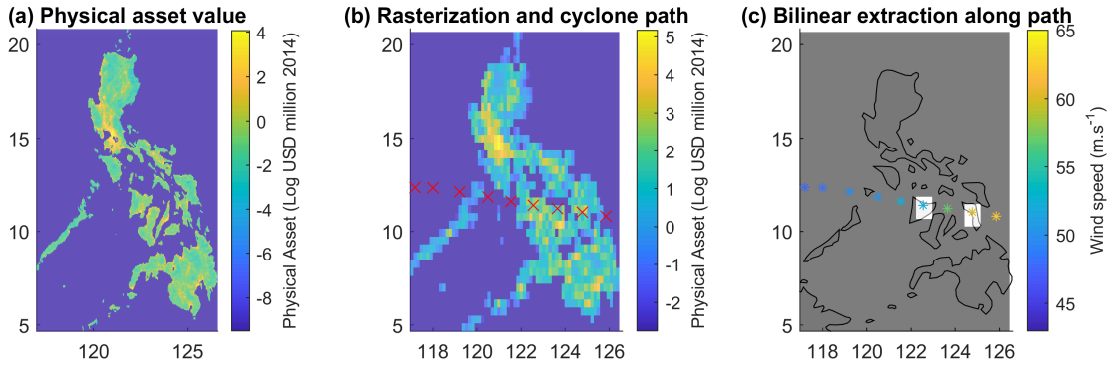

~~path~~

Figure 17. Illustration of the high resolution asset data (a) ~~rasterization~~ original physical asset value resolution; (b) ~~and interpolation process (c)~~ aggregation of asset value over 0.25° boxes to evaluate asset exposure along ~~tracks~~interpolated cyclone track (here corresponding to the 2013 Hayan cyclone); (c) Illustration of damage calculation: damage is aggregated over the white boxes which correspond to cyclone locations over land.

4.4 Simplified damage estimation along tracks

In the context of our national level assessment, we propose a simplified damage module. The simulated damage for a given cyclone – in both IBTrACS and our synthetic tracks – is computed using the following procedure for each individual cyclone. First, a uniform grid of physical asset value with step given by the average cyclone radius is defined on the map of affected area. The cyclone track is linearly interpolated, and the tiles affected by the cyclone (containing a part of the interpolated path) are identified (see Figure 17). Second, for each tile identified in the previous step, we retrieve the maximum wind speed V, and compute the proportion of wealth lost $f(V, v_h^j)$ using the relation (15) with the total damage ratio parameter given in Eberenz et al. (2021). Then, we compute the total simulated damage by aggregating the physical asset exposure multiplied by the proportion of wealth lost on each tile over all tiles affected by the cyclone.

As a result of this procedure, we obtain the total simulated damage $\mathrm{SED}_i(j,t)$ caused by the i-th cyclone in region j, simulated with climate variables for year t. Finally, the cyclone damage cost in region j and year t is simulated as follows:

$$\mathcal{D}(j,t) = \sum_i \mathrm{SED}_i(j,t), \tag{20}$$

where the sum is taken over all cyclones occurring in a given year. This procedure can then be repeated many times to obtain the distribution of annual cyclone damages and compute other statistics such as the mean and quantiles of this distribution.

The damage functions used in the second step are retrieved directly from the CLIMADA environment. These functions were fitted with the same physical asset value~~, however,~~ . However, in our case, we project these values on a coarser grid (first step), in such a way that the extraction is simplified for a large number of synthetic tracks in the context of the present global exercise. To ensure that the estimated damages produced with this simplification are consistent with the historical

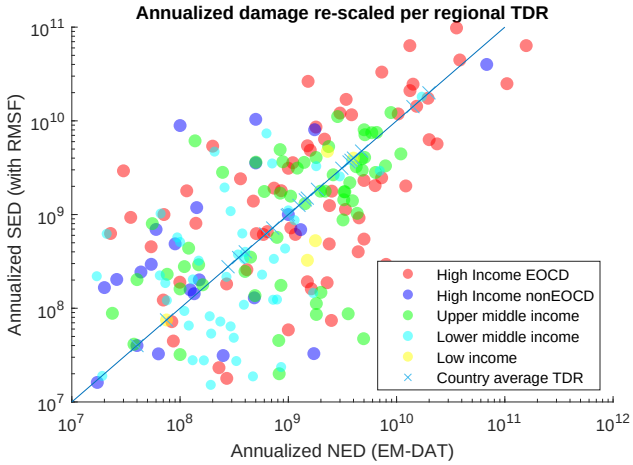

Figure 18. Estimated (RMSF) vs. reported damage. The filled dots represent individual ~~events~~ year/country pairs with reported damage in EM-DAT. The small targets represent countries average and large targets income groups average. This distribution is obtained using a 0.25 x 0.25 resolution projection. Crosses correspond to country average (over all years).

records, we computed simulated damages over the historical tracks and compared the results to EM-DAT. ~~Figure 18 presents the estimated versus actual damages computed using the TDR damage function.~~ We aggregate asset values on 0.25 x 0.25° grid. The ~~average estimation over realised~~ spread between SED and NRD distribution remains important. To further reduce the errors, we thus divide the simulated damage by the average estimated damage (SED) over realised damage (NRD) ratio in each region~~is acceptable, slightly overestimated for high income non-OECD countries (in particular for Taiwan), using the~~ , which are computed using the RMSF damage function on IBTrACS and total reported damage from EM-DAT~~.~~ :

$$\hat{r}_j = \frac{\sum_i \mathrm{SED}(i, v_h^{\mathrm{RMSF}}(j))}{\sum_i \mathrm{NRD}} \tag{21}$$

Figure 18 presents the estimated versus actual damages computed using the RMSF damage function and the distribution of the re-scaled estimation by country using the intersection of IBTrACS with lands (762 events), crossed with EMDAT (606). Each dot represents the total damage over a year in a country (211 observations).

~~Finally, the cyclone damage cost in region j and year~~

4.5 Dynamic projection of local exposure in SSPs

To estimate future exposures along the cyclone tracks in each scenario, we use the downscaled estimation for the exposed wealth (Eberenz et al., 2020) and the coefficients representing the change between the current state and the future scenario in the framework of the shared socioeconmic pathways (O'Neill et al., 2014, 2017; Jones and O'Neill, 2020). The local physical

exposure at the coordinates (x,y) at time t ~~is simulated~~ in a region j in scenario k is defined as follows:

$$\mathcal{D}(j,t) = \sum_i \mathrm{SED}_i(j,t),$$

$$\Phi(x,y,j,k,t) \approx \underbrace{F^{cap}_{\mathrm{GDP}}(j,k,t)}_{\text{Global macro factor}} \cdot \underbrace{F_{pop}(x,y,k,t) \cdot \mathcal{L}_P(x,y)}_{\text{Local factor}}. \tag{22}$$

where ~~the sum is taken over all cyclones occurring in a given year.This procedure can then be repeated many times to obtain the distribution of annual cyclone damages and compute other statistics such as the mean and quantiles of this distribution~~$\mathcal{L}_P(x,y)$ is the data from Eberenz et al. (2020). The factor F^{cap}_{GDP} is the projected GDP per capita growth for each region:

$$F^{cap}_{\mathrm{GDP}}(j,k,t) \approx \frac{\mathrm{GDP}(j,k,t)/\mathrm{GDP}(j,t=2020)}{P(j,k,t)/P(j,t=2020)} \tag{23}$$

where P is the total population of the region retrieved from SSP database (Riahi et al., 2017).[15] Figure 19 displays the scenario-based projections of GDP and population in the five SSP, at the regional level by the IIASA model. The population exposure growth factor F_{pop} is defined as follows:

$$F_{pop}(x,y,k,t) \approx \frac{p(x,y,k,t)}{p(x,y,t=2020)} \tag{24}$$

where $p(x,y,k,t)$ represents the local projections of population (Jones and O'Neill, 2020) illustrated in Figure 20.

5 Application to damage assessment in representative concentration pathways (RCP)

5.1 Climate simulation ~~debiaising~~ bias correction for climate change application

The variables from climate model projections used by CATHERINA are subject to multiple biases. To reduce uncertainty caused by these biases, we use the *Cumulative Distribution Function-transform* (CDF-t) method developed in ~~(Vrac et al., 2012; Michelang~~ Vrac et al. (2012); Michelangeli et al. (2009) to correct the distribution of each variable, in each basin. Our bias correction approach is the standard in the climate community (Navarro-Racines et al., 2020). [16]

Consider a generic climate variable (denoted by χ) at a fixed location, which is available both from ERA5 reanalysis and from a given CMIP5 model. We are interested in two time periods: the historical period (covered both by the climate model and the reanalysis) and a future time period (covered only by the climate model). Let F^h_{ERA5} and F^h_{CMIP} be the distribution functions of χ under reanalysis and under climate model for the historical period, and F^f_{CMIP5} be the distribution function of χ under climate model for the future period. The distribution function under the climate model is subject to much stronger biases

[15] https://tntcat.iiasa.ac.at/SspDb/.

[16] see http://ccafs-climate.org/bias_correction/

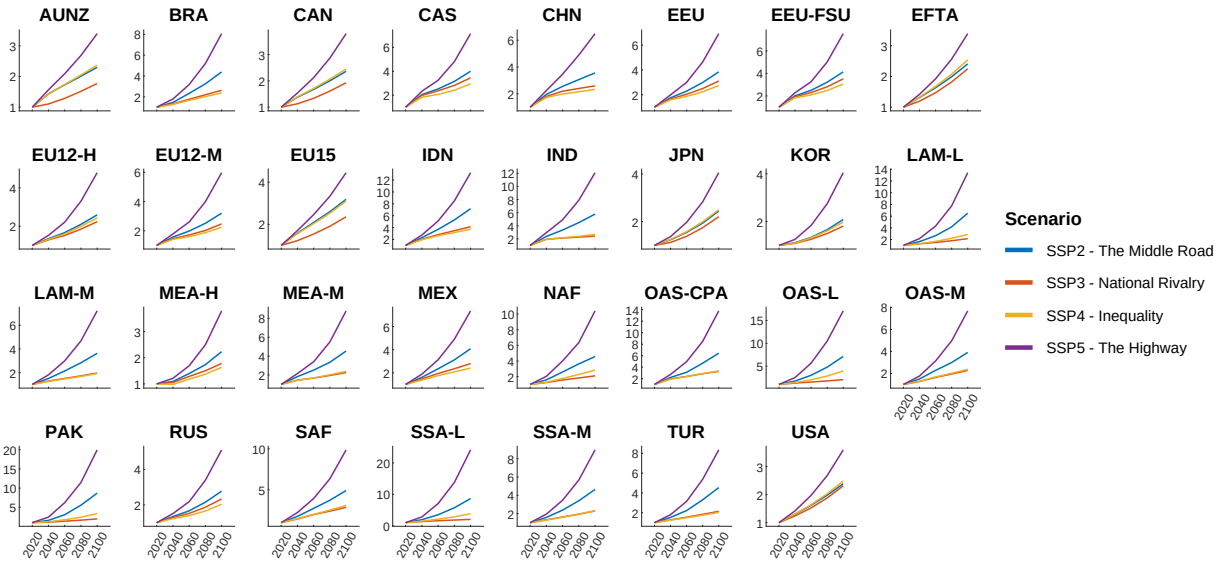

Figure 19. Regional F^{cap}_{GDP} factor variation in SSPs IIASA database (R32). Source : https://tntcat.iiasa.ac.at/SspDb/. The country mapping is provided in Table **??**.

than that under the reanalysis. The CDF-t method constructs the distribution function for χ with reduced bias for the future time period, denoted by $\widehat{F}^{f}_{\mathrm{CMIP}}$ and given by

$$\widehat{F}^{f}_{\mathrm{CMIP}}(\cdot) = F^{h}_{\mathrm{ERA5}}(F^{h,-1}_{\mathrm{CMIP}}(F^{f}_{\mathrm{CMIP}}(\cdot))),$$

$$\widehat{F}^{f}_{\mathrm{CMIP}}(\cdot) = F^{h}_{\mathrm{ERA5}}(F^{h,-1}_{\mathrm{CMIP}}(F^{f}_{\mathrm{CMIP}}(\cdot))),$$

where $F^{h,-1}_{\mathrm{CMIP}}$ is the inverse function of F^{h}_{CMIP}. For a given value χ^{f}_{CMIP} of the variable χ obtained for the future period from the climate model, the corresponding bias-corrected value $\hat{\chi}^{f}_{CMIP}$ may then be computed via

$$\begin{aligned}\hat{\chi}^{f}_{CMIP} &= \widehat{F}^{f,-1}_{\mathrm{CMIP}}(F^{f}_{\mathrm{CMIP}}) \\ &= F^{f,-1}_{\mathrm{CMIP}}(F^{h}_{\mathrm{CMIP}}(F^{h,-1}_{\mathrm{ERA5}}(F^{f}_{\mathrm{CMIP}}(\chi^{f}_{CMIP})))).\end{aligned}$$

When the future period and the historical period coincide, the method reduces to the standard quantile transform:

$$\hat{\chi}^{h}_{CMIP} = F^{h,-1}_{\mathrm{ERA5}}(F^{h}_{\mathrm{CMIP}}(\chi^{h}_{CMIP})). \tag{25}$$

First, we use the method on the historical period to compare the description of the ~~MPI~~ thermodynamic potential and wind speed with and without correction, so equation (25) may be used directly. To extract the CDFs of the variables of interest, we generate synthetic ~~tracks~~ track candidates from 1980 (beginning of ERA-5) to ~~2010~~[17]. 2010. We launch the simulation 10

[17] ~~We launch 10 times over these 30 years to obtain at least 300 representative years.~~

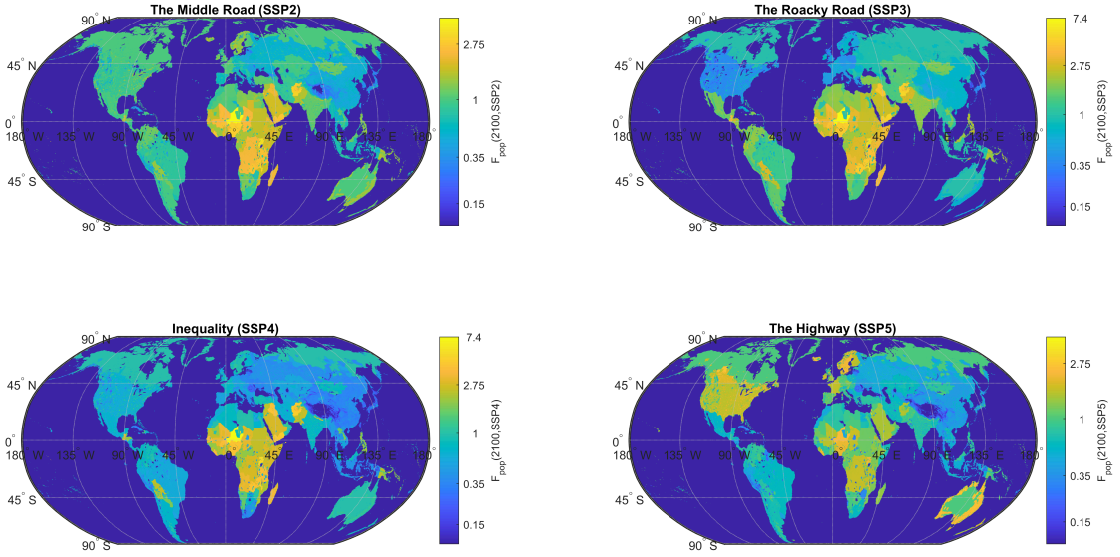

Figure 20. Local F_{pop} factor variation in all SSPs in 20100 (source: Jones and O'Neill (2020), NASA Socio-Economic Data Application Center (SEDAC)). The scenario-based population grid generation methodology is detailed by Jones and O'Neill (2020) with a last version downscaled at 1 km following Gao (2020). This population grid is available every 10 years. CATHERINA uses the closest value in the definition of the exposure.

times over these 30 years to obtain 300 representative years. By definition, for the genesis of the cyclones, the time of year and location are in line with historical cyclone data. However, in this module, the synthetic tracks are generated without climate constraints, i.e. cyclones are allowed to drift relatively far away from their genesis location (in the limits of their initial basin), and therefore can cover conditions which do not lead to the formation of tropical cyclones. At this stage, these tracks are not to be considered as 'tropical cyclone tracks' but as 'candidate' tracks. In the following stage, actual cyclone tracks will be generated from candidate tracks by filtering those ones where meteorological conditions for cyclone formation are satisfied. For each point in space and time along these synthetic tracks, we extract the values of the four climate variables from the reanalysis (ERA-5) and from the historical simulations of the 7 climate models. Then, by comparing the CDF of the climate variables estimated by the models with the reference CDF ~~compute~~ computed from the reanalysis~~for each grid point~~, we determine the transformation allowing the values estimated by the models to better match those from ERA-5. ~~Sea surface temperature (K) Sea level pressure (hPa) Relative humidity (%) Tropopause temperature (K) Cumulative distribution functions per basin for the variables of interest along synthetic tracks produced with ERA-5 and extracted (at the same location) from climate data~~

~~produced by the 7 climate models.NA: North America, EP: East Pacific, NI: North Indian, SI: South Indian, SP: South Pacific, WP: West Pacific.~~

~~Figure A7 shows the distribution of sea surface temperature (SST), surface pressure (MSLP), relative humidity (RH) and troposphere temperature (T_{tropo}) at the same point in time in the historical runs.~~ The sea-level pressure distributions are stable over basins and models. The tropospheric temperature and near surface relative humidity distributions depend largely on the basin and display evidence of non-negligible model uncertainty. The sea-surface temperature estimates along the same synthetic tracks in the historical period display much larger uncertainty. The North Indian basin presents the widest uncertainty for all climate variables, which adds further uncertainty concerning the impact of climate change on tropical cyclones in this area[17]~~.~~.[17]

Individual variables entering the MPI computation are correlated as shown in Table 3. For example, sea-surface temperature and tropopause temperature exhibit a negative correlation of 83%. Therefore, applying bias correction to individual variables may lead to unrealistic combinations when evaluating the thermodynamic potentials. For example, extremely low tropopause temperatures associated with very high SSTs lead to overemphasizing lapse rates therefore generating unrealistically large potentials. To overcome this issue we perform the bias correction on the MSLP, SST, thermodynamic efficiency factor $\mathcal{E}$, and relative humidity - which should not be correlated to other variable according to the level of correlation present in the reanalysis. Figure 21 shows that this correction leads to similar distribution of the thermodynamic potentials in the models and the reanalysis.

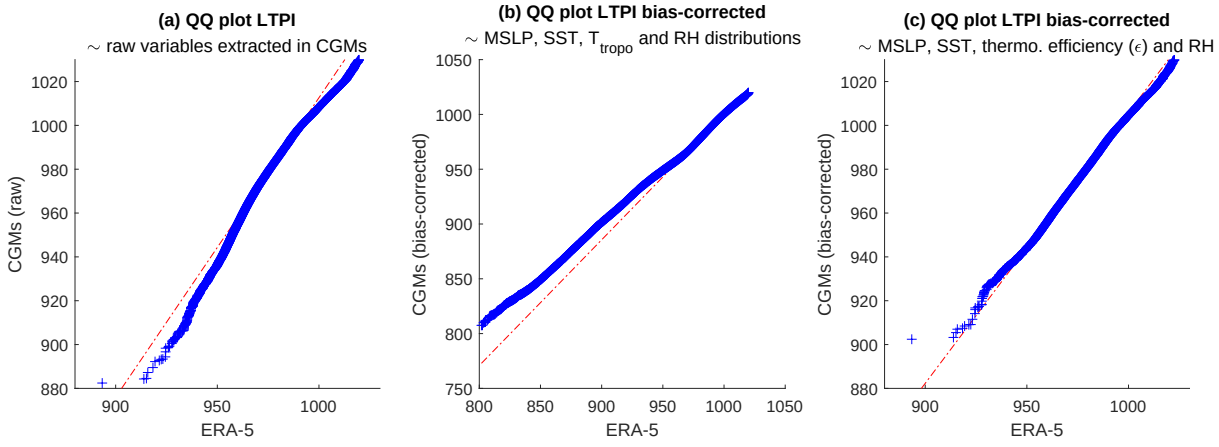

Figure 21. Bias correction module QQplots

We apply the CDF-t correction technique along our historical synthetic tracks and compute the maximum potential intensity following section 3.3.2. The pressure follows the dynamic process introduced in section 3.3.4 and the corresponding wind is derived from the WPR (see section 3.3.1). We define the model error as the relative error $\left(\frac{\chi_{\mathrm{CMIP}}-\chi_{\mathrm{ERA5}}}{\chi_{\mathrm{ERA5}}}\right)$ between the value produced by the model and the one produced by the reanalysis ERA-5. Figure 22 displays the average relative errors and

[17] ~~These biases and uncertainties may be mitigated in the latest launch of the models at the occasion of the CMIP6 (Gusain et al., 2020).~~

[17] Figure A7 presents the CDF-t of climate data in the sub-sample. These important biases and uncertainties may be mitigated in the latest launch of the models at the occasion of the CMIP6 (Gusain et al., 2020).

Table 3. Correlation levels (global) of modeled variables affecting the MPI with their reference values in ERA5

	SST_{ERA5}	SST_{CGMs}	$MSLP_{ERA5}$	$MSLP_{CGMs}$	T^{tropo}_{ERA5}	T^{tropo}_{CGMs}	RH_{ERA5}	RH_{CGMs}
SST_{ERA5}	1							
SST_{CGMs}	0.95	1						
$MSLP_{ERA5}$	0.46	0.39	1					
$MSLP_{CGMs}$	0.45	0.38	0.86	1				
T^{tropo}_{ERA5}	-0.83	-0.82	-0.37	-0.33	1			
T^{tropo}_{CGMs}	-0.77	-0.79	-0.31	-0.27	0.85	1		
RH_{ERA5}	-0.07	-0.07	-0.12	-0.09	0.22	0.19	1	
RH_{CGMs}	-0.27	-0.30	-0.18	-0.14	0.33	0.37	0.47	1

shows that a 42% relative error in the description of the maximum potential intensity can lead to ~~a 35~~more than 20% error in the description of the implied wind compared to the result obtained with ERA-5. ~~On~~ This figure illustrates the efficiency of bias correction in the historical period. Indeed, on average the CDF-t correction technique clearly reduces the error between the MPI estimated with climate reanalysis and the one computed from modeled climate data as well as (more importantly) the error in the description of the maximum wind speed. ~~In relative terms, the average relative error is reduced by more than 65% for the MPI and 74% for the wind.~~ However, running CATHERINA on the different CGMs still produces a wide range of results in climate projections (c.f. Figure 22). Although the intensity of the storms increases with each model, underlying climate modeling uncertainty still strongly impacts the synthetic tracks produced.

~~Relative error at the level of maximum potential intensity (MPI) and corresponding maximum wind speed computed with ERA-5 and climate data produced by the 7 climate models for the historical period. The transparent grey bars represent original errors and the color parts represent the residual relative error after CDF-t correction averaged over 30 years of cyclones.~~

5.2 Results in CMIP5 projections

The international climate modeling community introduced ~~shared socioeconomic~~ shared socioeconomic pathways (SSP) to translate varying narratives on the development of the society in the long-term. These projections impact the local physical asset value dynamics (Jones and O'Neill, 2020; Chen et al., 2020), and global macroeconomic variables (O'Neill et al., 2014, 2017). Under the ~~assumption of constant~~ assumptions of constant cyclone genesis frequency and constant impact ratio (i.e. the damage functions remain the same), CATHERINA allows us to derive damage projections in varying climate and socio-economic scenarios. Socio-economic change leads to wider differences than climate change, and this was expected (cf. Mendelsohn et al. (2012), Figure 3 for example). Using bias-corrected climate variable projections from the seven climate

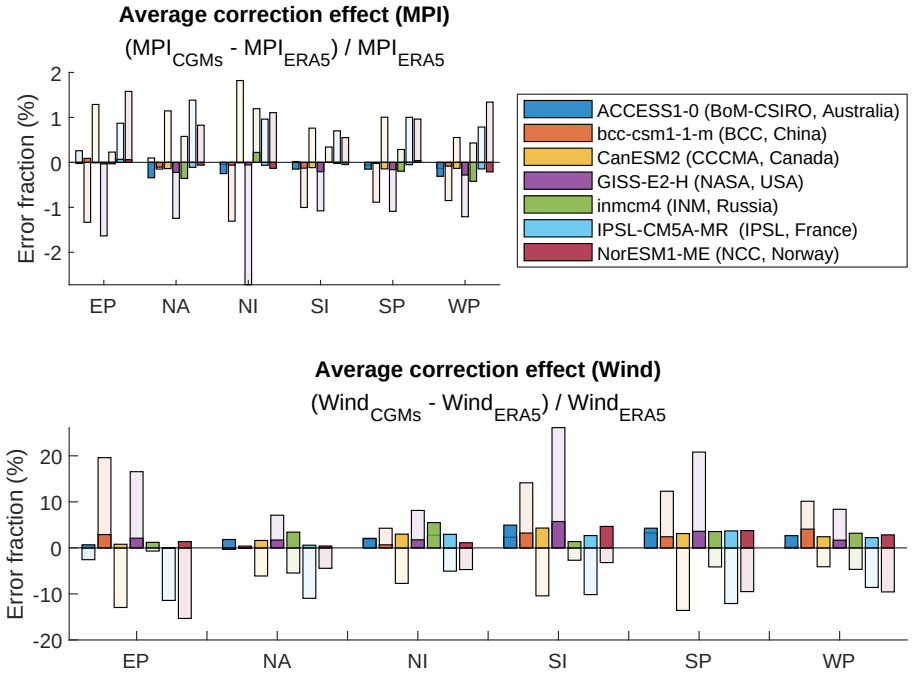

Figure 22. ~~Average and standard deviation~~ Relative error at the level of ~~max pressure drop and~~ maximum ~~wind speed generated~~ potential intensity (MPI) computed with ERA-5 and climate data produced by the ~~CMIP5~~ 7 climate models for the historical period. The transparent bars represent original errors and the color parts represent the residual relative error after CDF-t correction averaged over 30 years of cyclones.

models over the period 2070-2100, we provide an example of the application of the CATHERINA framework[18]~~.~~.[18] We run the model and produce synthetic tracks using climate projections of several models.

For example, over 2070-2100, the RCP 2.6 scenario, which is in line with the Paris Agreement and keeps global warming below 2°C by 2100, involves ~~an increase in~~ a growth of expected global annual financial losses ~~of 27%~~ from tropical cyclones by a factor of 4.84 on average compared to the last 40 years. In the case of RCP 4.5 (between 1.7 and 3.2°C warming by 2100) and RCP 8.5 (between 3.2 and 5.4°C warming by 2100), the average expected damage ~~increases respectively by 74% and 130%.~~ will be multiplied by 5.99 and 7.95 respectively. These results were obtained under the economic assumptions associated ~~to~~ with the socio-economic pathway SSP2 (i.e. the ~~"~~'*Middle of the Road*~~"~~' scenario in O'Neill et al. (2014)'s framework). The choice of the socio-economic scenario is also a determinant for damage estimation. In the case of the SSP5 socio-economic scenario (which assumes sustained exponential economic growth), with constant damage functions, the previous figures become ~~120%,~~

[18] ~~Because of the time slicing of the CMIP5 climate data available in the climate data store, we launch the models on 25 consecutive years over this period: 2070-2095 for IPSL, BCC, NCC, CCCMA, 2075-2100 for GISS, 2085-2095 for INM (only a 10 year slice of climate data is available on the CDS for this model). We repeat this process changing the seed 12 times to obtain 300 representative years in each model (except INM for which we only have 120 years).~~

[18] Because of the time slicing of the CMIP5 climate data available in the climate data store, we launch the models on 25 consecutive years over this period: 2070-2095 for IPSL, BCC, NCC, CCCMA, 2075-2100 for GISS and 2085-2095 for INM (only a 10 year slice of climate data is available on the CDS for this model). We repeat this process changing the seed 12 times to obtain 300 representative years in each model (except INM for which we only have 120 years).

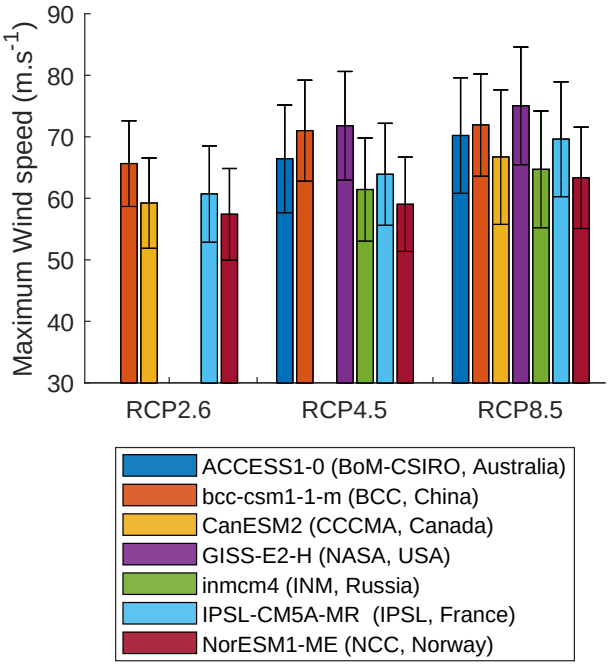

Figure 23. Average and standard deviation of maximum wind speed of tropical cyclones generated with the CMIP5 models after correction

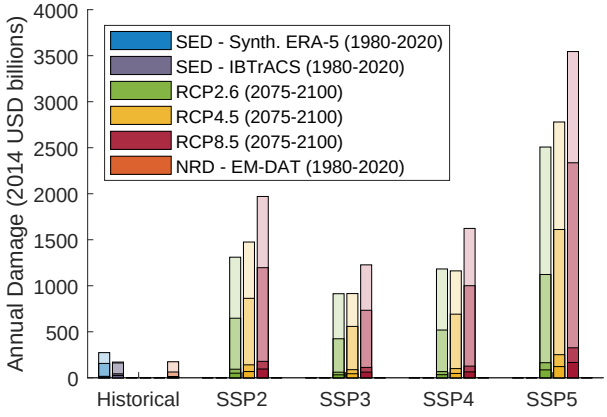

Figure 24. Annualized global damage in ~~shared-socioeconomic~~ shared socioeconomic pathways (SSP) and representative concentration pathways (RCP) between 2070 ~~an~~ and 2100 based on synthetic tracks produced with 7 climate models (with bias correction) over 250 representative years launched independently. Top range: ~~95% – 99%~~ 95% – 98% (*extremely unlikely* losses), followed by $95\% - 66\%$, $50\% - 66\%$ and $0\% - 50\%$. Historical damages are computed with 300 representative years of synthetic tracks generated with ERA-5 between 1980-2010. The physical asset value is corrected by inflation between cyclone year and 2014 (GDP ref. year of Litpop).

~~203% and 306% respectively.~~ 8.67, 11.1 and 15.22 respectively. Table 4 provides the expected values in the simulations and Figure 24 provides the quantile values for the modeled damage obtained using CATHERINA. At a global scale, in the SSP2 and

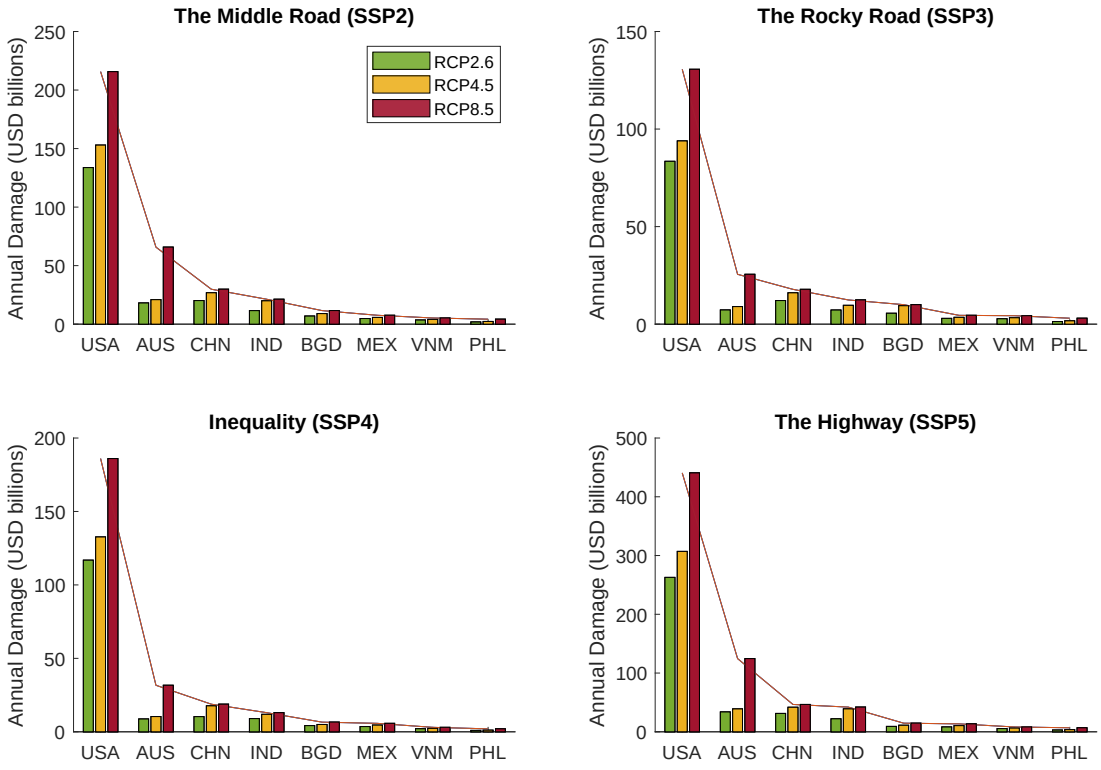

Figure 25. Annualized regional expected damage in SSP and RCP between 2070 an 2100 based on synthetic tracks produced with 7 climate models (with bias correction) over 250 representative years launched independently. The scale differs between SSPs.

the RCP 4.5 damages above USD 67.7 billion are '*more likely than not*', accounting for tropical cyclone related direct damage only. In the SSP5-RCP 8.5, the median losses establish at 166.3 USD billion in the current calibration of CATHERINA. We reiterate that the scale and spread of annual damage per country is sensitive to the scaling parameter that would benefit from more precise local calibration. However, the sensitivity to changing is present under all assumptions.

Figures 25 displays the average annual damage per country, in the different ~~shared-socioeconomic pathways.~~ shared socioeconomic pathways. We can see that the distributions across countries are slightly different from one SSP to another. Indeed, we have the same distribution in SSP2 and SSP5 with a higher expected damage in SSP5 because of the growth hypothesis this scenario relies on. However, SSP3 (rocky road) or SSP4 (inequality) are distributed differently. The scenario emphasizing inequalities – and its interpretation by scientists in terms of (i) socioeconomic developments Riahi et al. (2017) and (ii) population distribution Jones and O'Neill (2017) – increases damage concentration in the United-States. On the other hand, the rocky-road scenario, linked to a larger and more rural population, lower GDP and national rivalry sees the damage more equally distributed among other nations.

We ran the 7 models over 300 representative years to obtain these distributions. In these illustrative simulations, there is an effect due to certain large coastal cities exposure for the '*very unlikely*' band (between 95 to 98 percentile) of annual damages.

Table 4. Simulated expected annual damage (2014 USD Billions) in historical calibration period and representative concentration pathways between 2075 and 2100

SSP	Configuration and RCP	Mean damage USD Bn
Historical (1980-2020)	Synthetic ERA-5	34.72
Historical (1980-2020)	Computed along IBTrACS	47.59
Historical (1980-2020)	Reported in EM-DAT	21.10
SSP2	RCP26	164.81
SSP2	RCP45	208.23
SSP2	RCP85	276.36
SSP3	RCP26	105.51
SSP3	RCP45	133.66
SSP3	RCP85	172.20
SSP4	RCP26	128.77
SSP4	RCP45	161.95
SSP4	RCP85	216.12
SSP5	RCP26	301.78
SSP5	RCP45	385.36
SSP5	RCP85	528.41

However, given the scale observed more than one city have been hit by storms. Because the aim of the model was also to stress test the resiliency of the financial and economic systems, looking at the expected value of damage can be less interesting that studying the quantile value, especially in the context of events with large tail-risk. Coronese et al. (2019) investigating the increase in economic damage due to extreme natural disasters supports this thesis showing that the impact of climate change is particularly striking for extreme events (see for example, Coronese et al. (2019), Figure 2A).

6 Conclusions

This paper proposes a ~~relatively simple~~ novel structural framework to generate synthetic storms based on large-scale climate data and produce simulations of annual cyclone damages per country. We show that when used with reanalysis data and CMIP5 models over the historical period, our method produces tracks consistent with historical observations.

The synthetic tracks generated with our model have several applications. The first one is in natural disaster ~~risk management~~risk-managem to calibrate adaptation measures. For this purpose, the ~~track generation~~ track-generation algorithm may be enhanced, for instance, by including dependency in the latitudinal and longitudinal incremental displacement, coupling with a meteorological forecasting model, or including ground topography to model the cyclone displacement over land. Another major field of application is to climate financial risk management, where this scenario-based events database can be used to evaluate physical risks and compute portfolio exposures. This would require to better define asset-level vulnerabilities.

The dataset used for the examples of this paper, based on low resolution data and including a limited number of simulations, may not be accurate enough to properly calibrate adaptation measures. However, we believe that the framework presented here may be used to project a dense set of trajectories, compute expected damage and damage percentiles over the next decades and measure the investment required for adaptation and mitigation measures in the next fifty years. This work also reflects a practical exercise not carried out until now, of cross-referencing the latest data sets developed, putting into perspective both the socio-economic and climatic development hypotheses, and to carrying out a bottom-up, rather than top-down, damage calculation.

Code and data availability. Code is available from the E4C datahub at https://www.e4c.ip-paris.fr/#/fr/datahub/projects, and Zenodo at 10.5281/zenodo.5645516. The deposit includes R scripts with functions, a fitting script, the parameters of the fitting of all the relationships on ERA-5, historical and future synthetic tracks, and a sample of simulated annual damage per country and scenario. We included a user guide for data exploration and a quick start guide.

References

Arthur, W. C.: A statistical–parametric model of tropical cyclones for hazard assessment, Natural Hazards and Earth System Sciences, 21, 893–916, 2021.

Aznar Siguan, G. and Bresch, D. N.: CLIMADA v1: a global weather and climate risk assessment platform, Geoscientific Model Development, 12, 3085–3097, 2019.

Bister, M. and Emanuel, K. A.: Low frequency variability of tropical cyclone potential intensity 1. Interannual to interdecadal variability, Journal of Geophysical Research: Atmospheres, 107, ACL–26, 2002.

Bloemendaal, N., Haigh, I. D., de Moel, H., Muis, S., Haarsma, R. J., and Aerts, J. C.: Generation of a global synthetic tropical cyclone hazard dataset using STORM, Scientific Data, 7, 1–12, 2020.

Bresch, D. N.: CLIMADA-the open-source and-access global probabilistic risk modelling platform, 2017.

Bruyère, C., Holland, G., Prein, A., Done, J., Buckley, B., Chan, P., Leplastrier, M., and Dyer, A.: Severe weather in a changing climate, Insurance Australia Group and National Center for Atmospheric Research, November. https://www. iag. com. au/sites/default/files/documents/Severe-weather-in-a-changing-climate-report-011119. pdf, 2019.

Butchart, N., Austin, J., Knight, J. R., Scaife, A. A., and Gallani, M. L.: The response of the stratospheric climate to projected changes in the concentrations of well-mixed greenhouse gases from 1992 to 2051, Journal of climate, 13, 2142–2159, 2000.

Center for International Earth Science Information Network (CIESIN): Documentation for the gridded population of the world, Version 4 (GPWv4), Revision 10 Data Sets, 2017.

Chen, G., Li, X., Liu, X., Chen, Y., Liang, X., Leng, J., Xu, X., Liao, W., Wu, Q., Huang, K., et al.: Global projections of future urban land expansion under shared socioeconomic pathways, Nature communications, 11, 1–12, 2020.

Chen, Y., Gao, S., Li, X., and Shen, X.: Key Environmental Factors for Rapid Intensification of the South China Sea Tropical Cyclones, Frontiers in Earth Science, 8, 727, 2021.

Coronese, M., Lamperti, F., Keller, K., Chiaromonte, F., and Roventini, A.: Evidence for sharp increase in the economic damages of extreme natural disasters, Proceedings of the National Academy of Sciences, 116, 21 450–21 455, 2019.

Courtney, J.: Adapting the Knaff and Zehr wind-pressure relationship for operational use in Tropical Cyclone Warning Centres, Australian Meteorological and Oceanographic Journal, 58, 167, 2009.

Courtney, J. and Burton, A.: Joint Industry Project for Objective Tropical Cyclone Reanalysis: Final Report, Bureau of Meteorology, 87pp, 2018.

Courtney, J. B., Foley, G. R., van Burgel, J. L., Trewin, B., Burton, A. D., Callaghan, J., and Davidson, N. E.: Revisions to the Australian tropical cyclone best track database, Journal of Southern Hemisphere Earth Systems Science, 71, 203–227, 2021.

Credit Suisse: Credit Suisse Research Institute: Global Wealth Report 2017, https://www.credit-suisse.com/about-us-news/en/articles/news-and-expertise/global-wealth-report-2017-201711.html, 2017.

DeMaria, M. and Kaplan, J.: A statistical hurricane intensity prediction scheme (SHIPS) for the Atlantic basin, Weather and Forecasting, 9, 209–220, 1994.

DeMaria, M., Knaff, J. A., and Connell, B. H.: A tropical cyclone genesis parameter for the tropical Atlantic, Weather and Forecasting, 16, 219–233, 2001.

Eberenz, S., Stocker, D., Röösli, T., and Bresch, D. N.: LitPop: Global Exposure Data for Disaster Risk Assessment, 2019.

Eberenz, S., Stocker, D., Röösli, T., and Bresch, D. N.: Asset exposure data for global physical risk assessment, Earth Syst, 12, https://doi.org/10.5194/essd-12-817-2020, 2020.

Eberenz, S., Lüthi, S., and Bresch, D. N.: Regional tropical cyclone impact functions for globally consistent risk assessments, Natural Hazards and Earth System Sciences, 21, 393–415, 2021.

Emanuel, K., Sundararajan, R., and Williams, J.: Hurricanes and global warming: Results from downscaling IPCC AR4 simulations, Bulletin of the American Meteorological Society, 89, 347–368, 2008.

Emanuel, K. A.: The maximum intensity of hurricanes, Journal of the Atmospheric Sciences, 45, 1143–1155, 1988.

Emanuel, K. A.: The theory of hurricanes, Annual Review of Fluid Mechanics, 23, 179–196, 1991.

Emanuel, K. A.: Thermodynamic control of hurricane intensity, Nature, 401, 665–669, 1999.

Emanuel, K. A.: Increasing destructiveness of tropical cyclones over the past 30 years, Nature, 436, 686–688, 2005.

Emanuel, K. A.: Global warming effects on US hurricane damage, Weather, Climate, and Society, 3, 261–268, 2011.

Fabregat, A., Mezic, I., and Poje, A. C.: Finite-time partitions for lagrangian structure identification in Gulf Stream eddy transport, arXiv preprint arXiv:1606.07382, 2016.

Forster, P. M., Bodeker, G., Schofield, R., Solomon, S., and Thompson, D.: Effects of ozone cooling in the tropical lower stratosphere and upper troposphere, Geophysical Research Letters, 34, 2007.

Gao, J.: Downscaling global spatial population projections from 1/8-degree to 1-km grid cells, Technical Notes NCAR, National Center for Atmospheric Researcher, Boulder, CO., USA, https://doi.org/10.7927/q7z9-9r69, 2020.

Geiger, T., Gütschow, J., Bresch, D. N., Emanuel, K., and Frieler, K.: Double benefit of limiting global warming for tropical cyclone exposure, Nature Climate Change, 11, 861–866, 2021.

Gidden, M. J., Riahi, K., Smith, S. J., Fujimori, S., Luderer, G., Kriegler, E., van Vuuren, D. P., van den Berg, M., Feng, L., Klein, D., Calvin, K., Doelman, J. C., Frank, S., Fricko, O., Harmsen, M., Hasegawa, T., Havlik, P., Hilaire, J., Hoesly, R., Horing, J., Popp, A., Stehfest, E., and Takahashi, K.: Global emissions pathways under different socioeconomic scenarios for use in CMIP6: a dataset of harmonized emissions trajectories through the end of the century, Geoscientific Model Development, 12, 1443–1475, https://doi.org/10.5194/gmd-12-1443-2019, 2019.

Gray, W. M.: Tropical cyclone genesis, Atmospheric science paper; no. 234, 1975.

Guha-Sapir, D., Below, R., and Hoyois, P.: EM-DAT: the CRED/OFDA international disaster database, 2018.

Gusain, A., Ghosh, S., and Karmakar, S.: Added value of CMIP6 over CMIP5 models in simulating Indian summer monsoon rainfall, Atmospheric Research, 232, 104 680, 2020.

Hall, T. M. and Jewson, S.: Statistical modelling of North Atlantic tropical cyclone tracks, Tellus A: Dynamic Meteorology and Oceanography, 59, 486–498, 2007.

Harper, B.: Tropical cyclone parameter estimation in the Australian Region, Systems Engineering Australia Pty Ltd for Woodside Energy Ltd, Perth, 83, 2002.

Hersbach, H., Bell, B., Berrisford, P., Hirahara, S., Horányi, A., Muñoz-Sabater, J., Nicolas, J., Peubey, C., Radu, R., Schepers, D., et al.: The ERA5 global reanalysis, Quarterly Journal of the Royal Meteorological Society, 146, 1999–2049, 2020.

Holland, G. J.: The maximum potential intensity of tropical cyclones, Journal of the atmospheric sciences, 54, 2519–2541, 1997.

James, M. and Mason, L.: Synthetic tropical cyclone database, Journal of waterway, port, coastal, and ocean engineering, 131, 181–192, 2005.

James, M. and Mason, L.: Closure to "Synthetic Tropical Cyclone Database" by MK James and LB Mason, Journal of Waterway, Port, Coastal, and Ocean Engineering, 132, 502–503, 2006.

Jien, J. Y., Gough, W. A., Butler, K., Cheng, V., and Arhonditsis, G.: Near-Time Sea Surface Temperature and Tropical Cyclone Intensity in the Eastern North Pacific Basin, in: Hurricanes and Climate Change, pp. 55–89, Springer, 2017.

Jones, B. and O'Neill, B.: Global Population Projection Grids Based on Shared Socioeconomic Pathways (SSPs), 2010-2100, Socioecon. Data Appl., 2017.

Jones, B. and O'Neill, B. C.: Global One-Eighth Degree Population Base Year and Projection Grids Based on the Shared Socioeconomic Pathways, Palisades, 2020.

Kaplan, J. and DeMaria, M.: A simple empirical model for predicting the decay of tropical cyclone winds after landfall, Journal of applied meteorology, 34, 2499–2512, 1995.

Knapp, K. R., Kruk, M. C., Levinson, D. H., Diamond, H. J., and Neumann, C. J.: The international best track archive for climate stewardship (IBTrACS) unifying tropical cyclone data, Bulletin of the American Meteorological Society, 91, 363–376, 2010.

Knutson, T., Camargo, S. J., Chan, J. C., Emanuel, K., Ho, C.-H., Kossin, J., Mohapatra, M., Satoh, M., Sugi, M., Walsh, K., et al.: Tropical cyclones and climate change assessment: Part II: Projected response to anthropogenic warming, Bulletin of the American Meteorological Society, 101, E303–E322, 2020.

Kossin, J. P.: A global slowdown of tropical-cyclone translation speed, Nature, 558, 104–107, 2018.

Kossin, J. P., Emanuel, K. A., and Vecchi, G. A.: The poleward migration of the location of tropical cyclone maximum intensity, Nature, 509, 349–352, 2014.

Leckebusch, G. C., Ulbrich, U., Fröhlich, L., and Pinto, J. G.: Property loss potentials for European midlatitude storms in a changing climate, Geophysical Research Letters, 34, 2007.

Lee, C.-Y., Tippett, M. K., Sobel, A. H., and Camargo, S. J.: An environmentally forced tropical cyclone hazard model, Journal of Advances in Modeling Earth Systems, 10, 223–241, 2018.

Lüthi, S.: Applying Machine Learning Methods to the Assessment of Tropical Cyclone Impacts, Master thesis, ETH Zurich, 2019.

Mendelsohn, R., Emanuel, K., Chonabayashi, S., and Bakkensen, L.: The impact of climate change on global tropical cyclone damage, Nature climate change, 2, 205–209, 2012.

Merrill, R. T.: An experiment in statistical prediction of tropical cyclone intensity change, vol. 34, US Department of Commerce, National Oceanic and Atmospheric Administration, 1987.

Michelangeli, P.-A., Vrac, M., and Loukos, H.: Probabilistic downscaling approaches: Application to wind cumulative distribution functions, Geophysical Research Letters, 36, 2009.

Navarro-Racines, C., Tarapues, J., Thornton, P., Jarvis, A., and Ramirez-Villegas, J.: High-resolution and bias-corrected CMIP5 projections for climate change impact assessments, Scientific data, 7, 1–14, 2020.

Neu, U., Akperov, M. G., Bellenbaum, N., Benestad, R., Blender, R., Caballero, R., Cocozza, A., Dacre, H. F., Feng, Y., Fraedrich, K., et al.: IMILAST: A community effort to intercompare extratropical cyclone detection and tracking algorithms, Bulletin of the American Meteorological Society, 94, 529–547, 2013.

O'Neill, B. C., Kriegler, E., Riahi, K., Ebi, K. L., Hallegatte, S., Carter, T. R., Mathur, R., and van Vuuren, D. P.: A new scenario framework for climate change research: the concept of shared socioeconomic pathways, Climatic change, 122, 387–400, 2014.

O'Neill, B. C., Kriegler, E., Ebi, K. L., Kemp-Benedict, E., Riahi, K., Rothman, D. S., van Ruijven, B. J., van Vuuren, D. P., Birkmann, J., Kok, K., et al.: The roads ahead: Narratives for shared socioeconomic pathways describing world futures in the 21st century, Global environmental change, 42, 169–180, 2017.

Pachauri, R. K., Allen, M. R., Barros, V. R., Broome, J., Cramer, W., Christ, R., Church, J. A., Clarke, L., Dahe, Q., Dasgupta, P., et al.: Climate change 2014: synthesis report. Contribution of Working Groups I, II and III to the fifth assessment report of the Intergovernmental Panel on Climate Change, Ipcc, 2014.

Prahl, B. F., Rybski, D., Burghoff, O., and Kropp, J. P.: Comparison of storm damage functions and their performance, Nat. Hazards Earth Syst. Sci., 15, 769–788, 2015.

Ramaswamy, V., Schwarzkopf, M., Randel, W., Santer, B., Soden, B. J., and Stenchikov, G.: Anthropogenic and natural influences in the evolution of lower stratospheric cooling, Science, 311, 1138–1141, 2006.

Riahi, K., van Vuuren, D. P., Kriegler, E., Edmonds, J., O'Neill, B. C., Fujimori, S., Bauer, N., Calvin, K., Dellink, R., Fricko, O., Lutz, W., Popp, A., Cuaresma, J. C., KC, S., Leimbach, M., Jiang, L., Kram, T., Rao, S., Emmerling, J., Ebi, K., Hasegawa, T., Havlik, P., HumpenÃ¶der, F., Silva, L. A. D., Smith, S., Stehfest, E., Bosetti, V., Eom, J., Gernaat, D., Masui, T., Rogelj, J., Strefler, J., Drouet, L., Krey, V., Luderer, G., Harmsen, M., Takahashi, K., Baumstark, L., Doelman, J. C., Kainuma, M., Klimont, Z., Marangoni, G., Lotze-Campen, H., Obersteiner, M., Tabeau, A., and Tavoni, M.: The Shared Socioeconomic Pathways and their energy, land use, and greenhouse gas emissions implications: An overview, Global Environmental Change, 42, 153–168, https://doi.org/10.1016/j.gloenvcha.2016.05.009, 2017.

Riahi, K., Bertram, C., Huppmann, D., Rogelj, J., Bosetti, V., Cabardos, A.-M., Deppermann, A., Drouet, L., Frank, S., Fricko, O., et al.: Cost and attainability of meeting stringent climate targets without overshoot, Nature Climate Change, 11, 1063–1069, 2021.

Rogelj, J., Popp, A., Calvin, K. V., Luderer, G., Emmerling, J., Gernaat, D., Fujimori, S., Strefler, J., Hasegawa, T., Marangoni, G., Krey, V., Kriegler, E., Riahi, K., van Vuuren, D. P., Doelman, J., Drouet, L., Edmonds, J., Fricko, O., Harmsen, M., Havlík, P., HumpenÃ¶der, F., Stehfest, E., and Tavoni, M.: Scenarios towards limiting global mean temperature increase below 1.5 °C, Nature Climate Change, 8, 325–332, https://doi.org/10.1038/s41558-018-0091-3, 2018.

Román, M. O., Wang, Z., Sun, Q., Kalb, V., Miller, S. D., Molthan, A., Schultz, L., Bell, J., Stokes, E. C., Pandey, B., et al.: NASA's Black Marble nighttime lights product suite, Remote Sensing of Environment, 210, 113–143, 2018.

Sherwood, S. C., Ingram, W., Tsushima, Y., Satoh, M., Roberts, M., Vidale, P. L., and O'Gorman, P. A.: Relative humidity changes in a warmer climate, Journal of Geophysical Research: Atmospheres, 115, 2010.

Solomon, S., Manning, M., Marquis, M., Qin, D., et al.: Climate change 2007-the physical science basis: Working group I contribution to the fourth assessment report of the IPCC, vol. 4, Cambridge university press, 2007.

Taylor, K. E., Stouffer, R. J., and Meehl, G. A.: An overview of CMIP5 and the experiment design, Bulletin of the American meteorological Society, 93, 485–498, 2012.

Unanwa, C., McDonald, J., Mehta, K., and Smith, D.: The development of wind damage bands for buildings, Journal of Wind Engineering and Industrial Aerodynamics, 84, 119–149, 2000.

Vrac, M., Drobinski, P., Merlo, A., Herrmann, M., Lavaysse, C., Li, L., and Somot, S.: Dynamical and statistical downscaling of the French Mediterranean climate: uncertainty assessment, Natural Hazards and Earth System Sciences, 12, 2769–2784, 2012.

World Bank: Building the World Bank's Wealth Accounts: Methods and Data, https://development-data-hub-s3-public.s3.amazonaws.com/ddhfiles/94641/wealth-methodology-january-30-2018_4_0.pdf, 2018.

World Bank: World Bank Open Data, available at, https://data.worldbank.org/, 2019.

Acknowledgements. This work contributes to the Energy4Climate Interdisciplinary Center (E4C) of Institut Polytechnique de Paris and Ecole des Ponts ParisTech, supported by 3rd Programme d'Investissements d'Avenir [ANR-18-EUR-0006-02]. Peter Tankov gratefully acknowledges financial support from the FIME Research Initiative. The authors are very grateful to Florian Raymond, Thierry Roncalli, Takaya Sekine and Lauren Stagnol for helpful comments.

Algorithm 1 Cyclone generation algorithm

$V \leftarrow 20\ \mathrm{m.s}^{-1}$

$P_c(s=0) \leftarrow \mathrm{MSLP} - \left(\frac{V}{a}\right)^{1/b}$

if $\mathrm{MSLP} - P_c > 0$ & $V > v_m$ & $s_l < 4$ **then**

while the pressure is bellow normal, wind is above threshold and we are not on land, do:

$$
\begin{aligned}
x(s) &\leftarrow x(s-1) + \Delta x(s) \\
\text{where} \quad & \Delta x(s) \propto \text{Equation (2)} \\
y(s) &\leftarrow y(s-1) + \Delta y(s) \\
\text{where} \quad & \Delta y_t \propto \text{Equation (3)} \\
\mathrm{MPI}(s) &\leftarrow \mathrm{f_{MPI}}(y(s), P_c(s-1), \mathrm{SST}(s), \\
& \quad T_{\mathrm{tropo}}(s), \mathrm{MSLP}(s), \mathrm{RH}(s)) \\
& \quad \mathrm{f_{MPI}} \propto \text{Equation (5)} \\
P_c(s) &\leftarrow \max(P_c(s) + \Delta P_c(s), \mathrm{MSLP}(s) - \mathrm{MPD}(s)) \\
& \quad \mathrm{MPD} \propto \text{Equation (11) \&} \\
& \quad \Delta P_c(s) \propto \text{Equation (12)} \\
V(s) &\leftarrow a\left(\mathrm{MSLP} - P_c(s)\right)^b
\end{aligned}
$$

if on land = TRUE **then**

$s_l \leftarrow s_l + 1$

end if

else

if $s_l > 4$ **then**

Same functional for x and y but, compute distance to land $D(s)$ from natural earth coastlines and do

$$
\begin{aligned}
V(s) &\leftarrow V_b + (R \cdot V_0 - V_b) e^{-\alpha s_l} \\
&- f_1(t_L)\left(\ln \frac{D}{D_0}\right) + f_2(t_L) \\
& \quad V(s) \propto \text{Equation (14)}
\end{aligned}
$$

$s_l \leftarrow s_l + 1$

end if

end if

Note: This algorithm assumes step-wise extraction of climate data in the Monte-Carlo process. Another way, closer to the framework suggested in Bloemendaal et al. (2020) would be to (i) compute the tracks without properties, (ii) retrieve all climate variables, (iii) determine the properties using the extracted climate conditions in the last step.

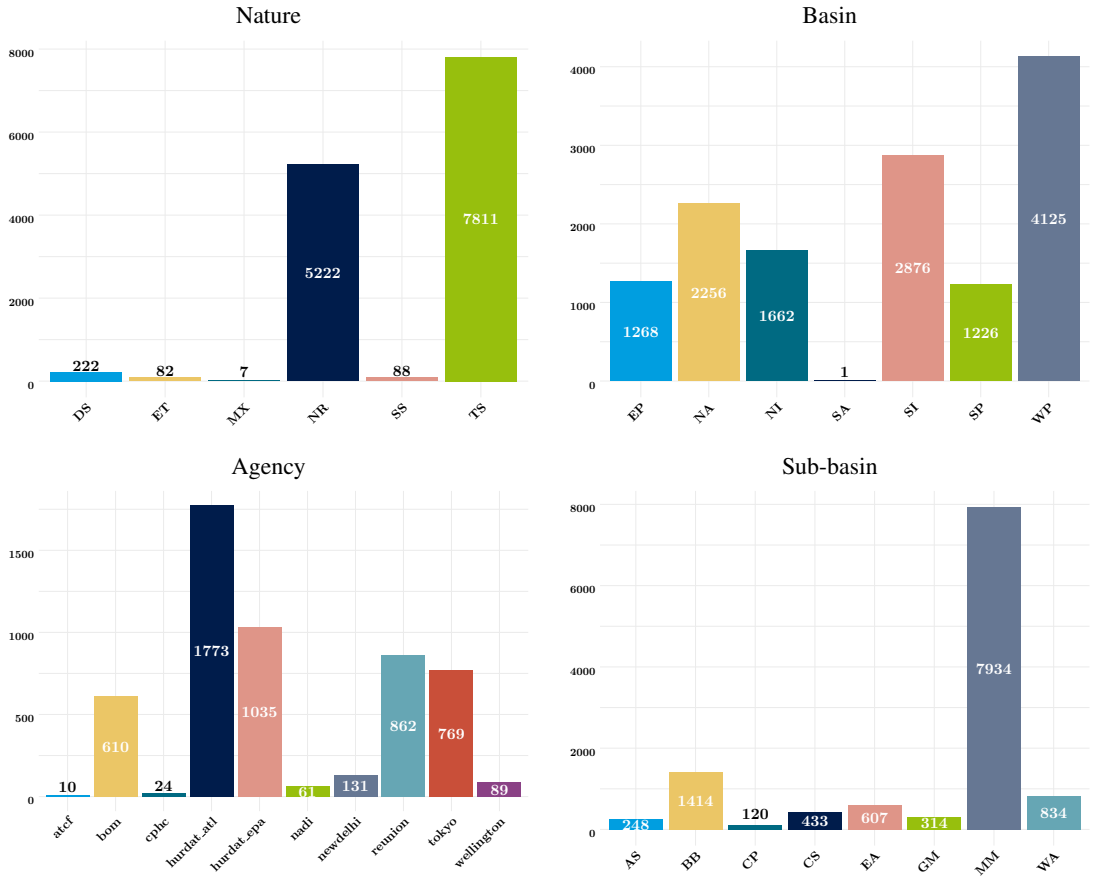

Figure A1. Information in IBTrACS.The cyclones are split by nature (DS: Disturbance; TS: Tropical; TE: Extratropical; ST: Subtropical; NR: Not reported; MX: Mixture or contradicting nature reports from different agencies). We remove Extratropical cyclones (75) and Disturbance (205). The cyclones are reported in the following basins: East Pacific (EP); North America (NA); North India (NI); South ~~America~~ Atlantic (SA); South India (SI); South Pacific (SP); Western Pacific (WP). One can also explore sub-basin decomposition Eberenz et al. (2021) (MM : missing - no sub basin for this basin (no sub-basins provided for WP, SI); CS : Caribbean Sea; GM : Gulf of Mexico; CP : Central Pacific; BB : Bay of Bengal; AS : Arabian Sea; WA : Western Australia; EA : Eastern Australia) but we chose to use basins. The different agencies worldwide report central pressure and maximum wind speed but use sometimes different standards. In particular, the reporting can vary in terms of sustained wind speed. According to the dataset documentation the North Atlantic - U.S. Miami (NOAA NHC) bureau (hurdat/atcf) gives the 1-minute winds speed while Tokyo i.e. RSMC Tokyo (JMA) provides dirrectly the 10-minute sustained wind speed (Similarly, newdelhi corresponding to RSMC New Delhi (IMD) gives the 3-minute wind speed; reunion - RSMC La Reunion (MFLR), the Australian TCWCs (TCWC Perth, Darwin, Brisbane) (BOM), the RSMC Nadi (FMS); TCWC Wellington (NZMS) provide the 10 minute sustained wind speed and (CMA) 2-minute sustained wind). The lack of reporting standards between agencies is a source of uncertainty in the input data.

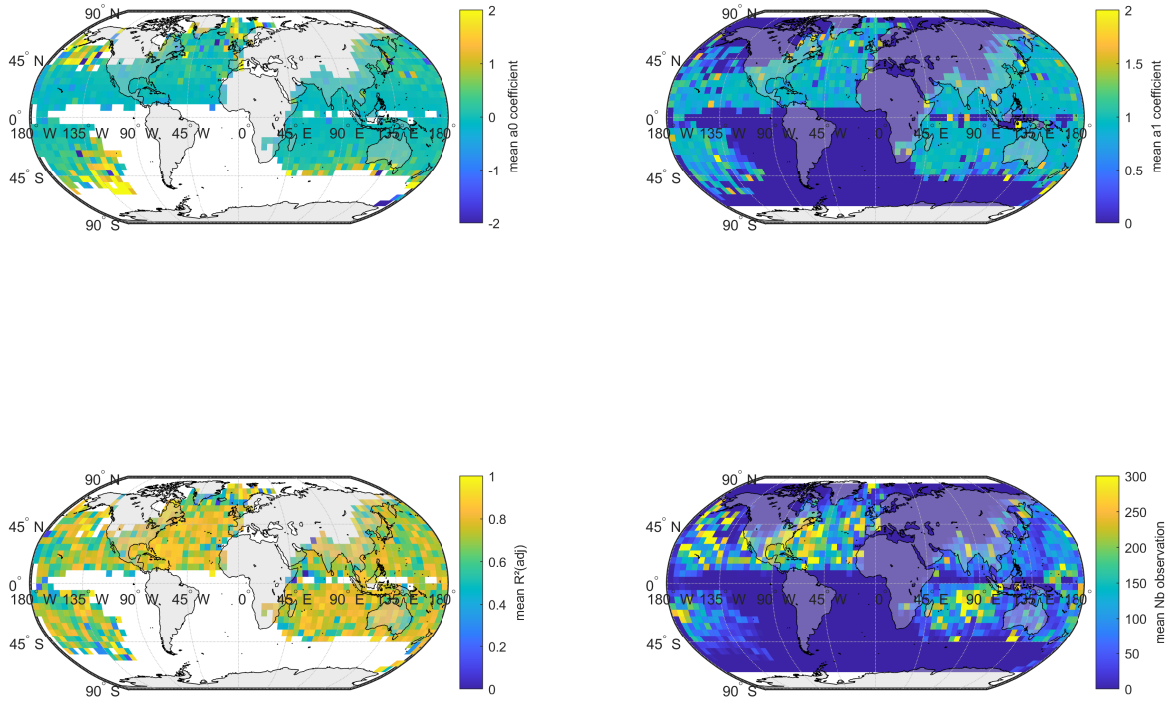

Figure A2. ~~IBTrACS full database tracks~~Map of longitude variation mean coefficients fitted on a 5x5 grid grouped per month

~~Simulated damage quantiles distributions per model per scenario (historical is restricted to ERA- for visualisation purpose). 0-50percentiles, 50-66 percentiles 66-95 and 95 to 99 percentiles are represented.~~

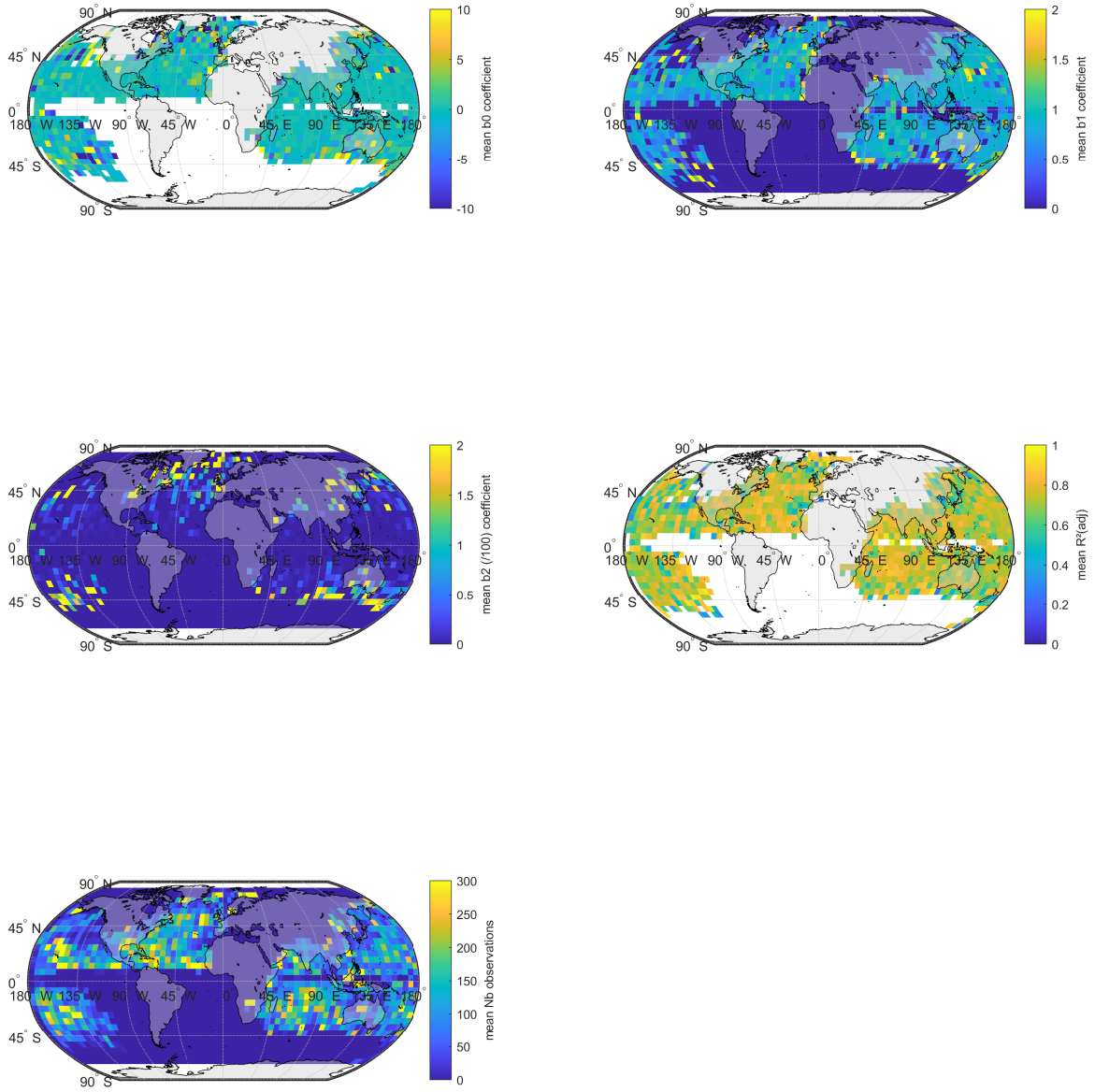

Figure A3. ~~Depression and sea surface temperature~~Map of latitude variation mean coefficients fitted on a 5x5 grid grouped per month

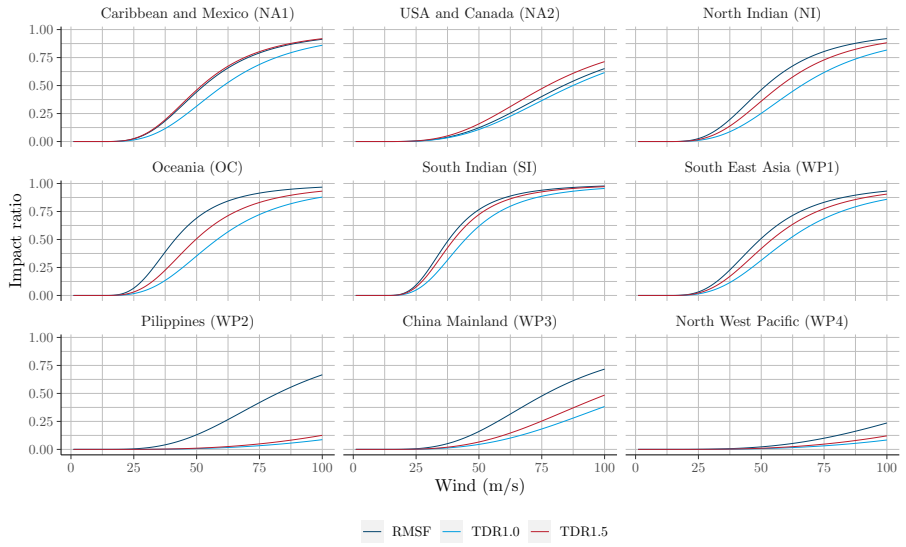

Figure A4. Regional Optimal Damage Functions of the CLIMADA package (Eberenz et al., 2021)

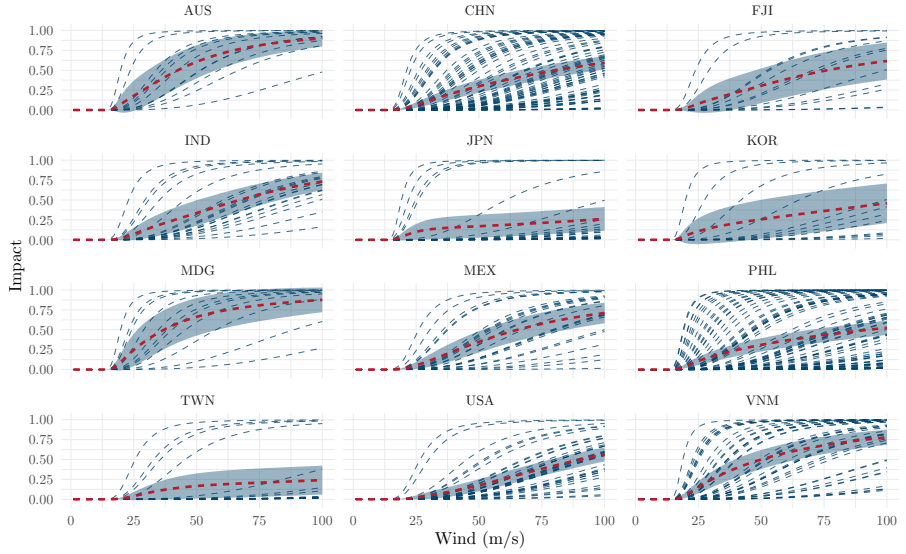

Figure A5. Country calibration of damage function (when the countries has been hit more than 5 times)

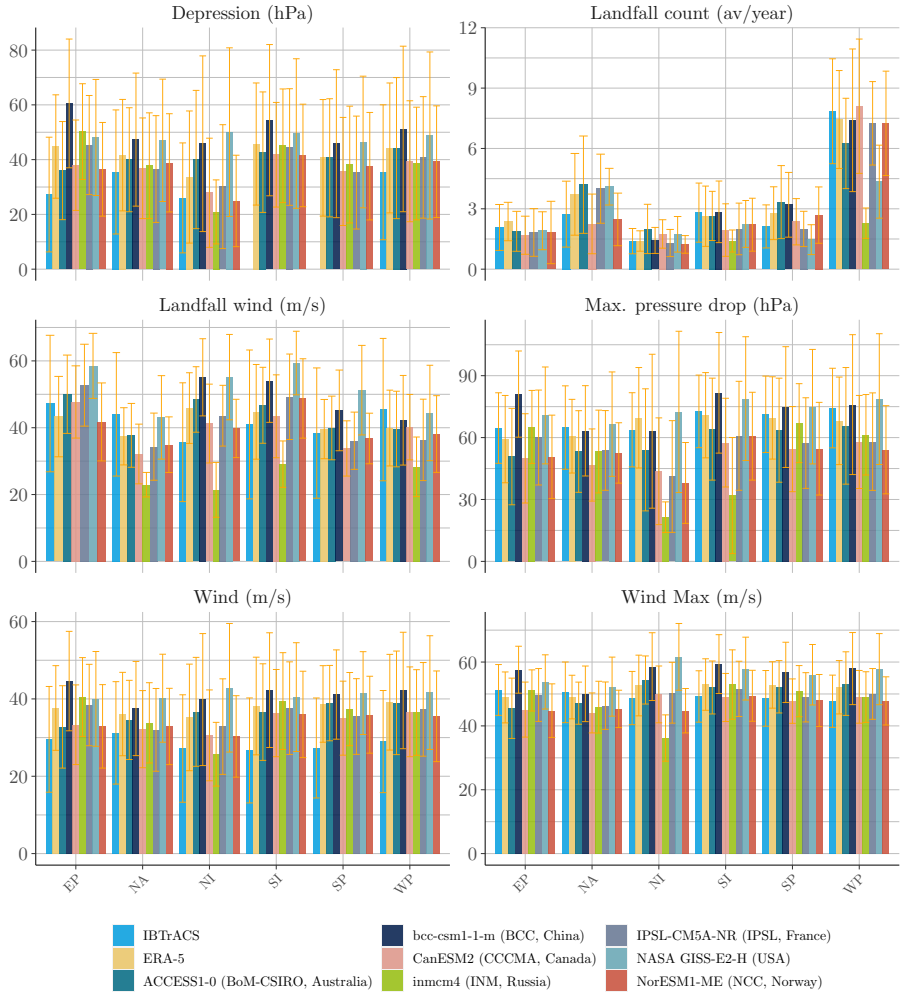

Figure A6. Evidence of models uncertainty. A comparison of the properties obtained generating 30 years of tropical cyclones with different models from the CMIP5 raw climate data versus ERA-5. The average number of cyclone making landfall is computed averaging the number of event with a number of steps on land positive ($s_l > 0$). Maximum pressure drop and wind are respectively computed extracting the maximum value for the corresponding variables of the cyclone tracks.The light blue bars represent the mean of the variable of interest among IBTrACS filtered dataset (with the confidence interval drawn from the standard deviation of the distribution). The yellow bars represent the same variable extracted from the synthetic data generated by the algorithm 1 using ERA-5 data. In terms of average values the models produce consistent tracks on every basins. Then, we compare the output of this algorithm with different climate data produced on the historical by the climate models taking part of the 5^{th} phase of the CMIP. A general observation is the poorer performance of the model in the North Indian basin. This could be due to the smaller number of intense cyclones remaining in the sample after the filtration by intensity (1.6 storms per year with wind exceeding 35 $\mathrm{m.s}^{-1}$).

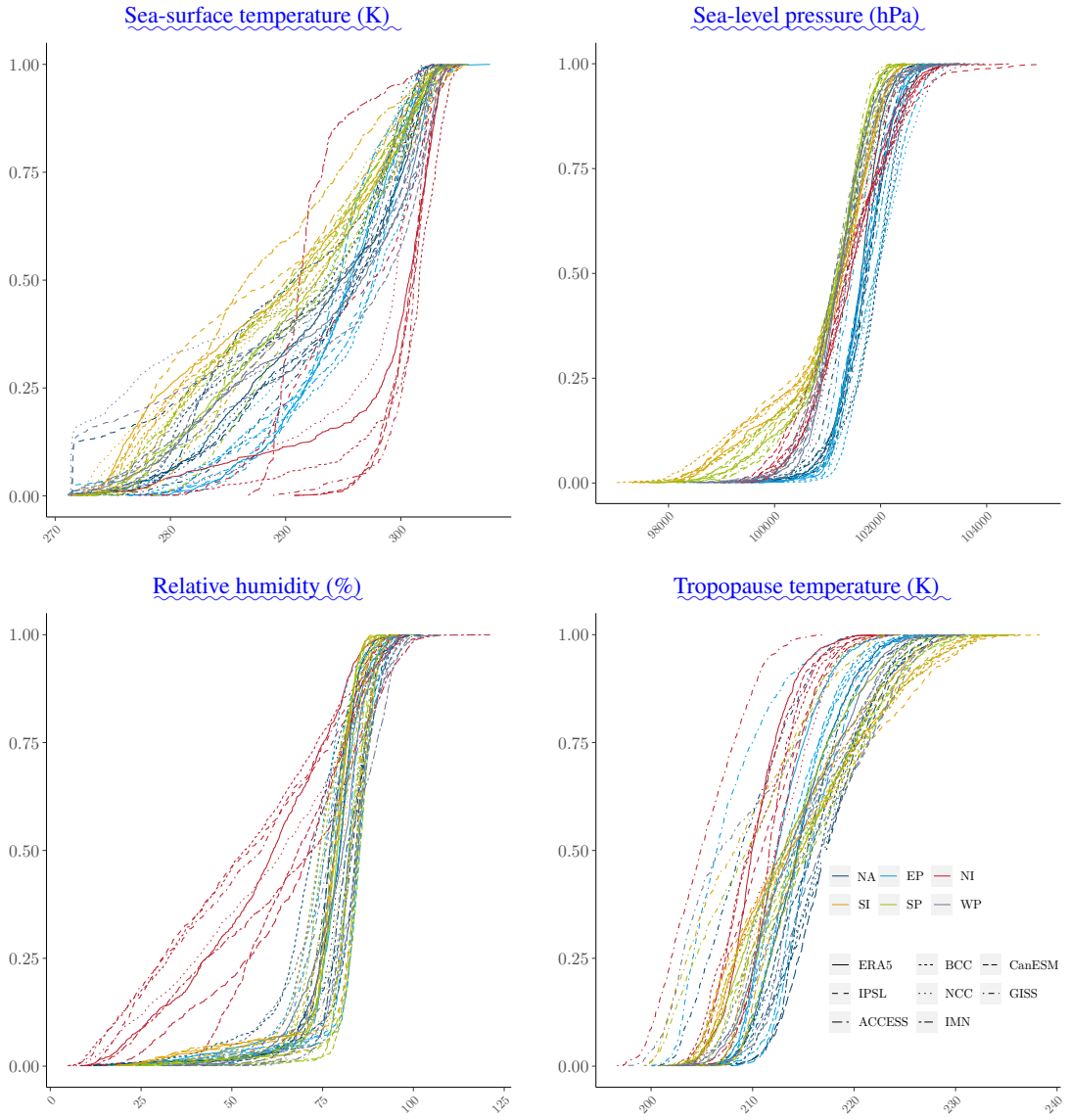

Figure A7. ~~Bias correction (300 years~~ Cumulative distribution functions per basin for the variables of interest along synthetic tracks produced with ERA-5 and extracted (at the same location) ~~. On~~ from climate data produced by the ~~top grid~~7 climate models.
NA: North America, ~~we compare Depression (hPa)~~EP: East Pacific, ~~landfall count and winds~~NI: North Indian, SI: South Indian, SP: South Pacific, WP: West Pacific.
The bias-correction module is indeed fitted on ~~the full sample~~a larger range of climate conditions. ~~We can see that~~ By definition, for the ~~correction effectively centers~~ genesis of the ~~distribution~~ cyclones, the time of ~~ERA-5 properties. The grid bellow focuses on a grouping on maximum wind~~ year and ~~depressions~~location are in line with historical cyclone data. ~~We note that~~ However, in the ~~correction also allows us~~ bias-correction module, the synthetic tracks are generated without climate constraints, i.e. cyclones are allowed to ~~reduce~~ drift relatively far away from their genesis location (in the ~~dispersion between models~~limits of their initial basin), ~~however~~and therefore can cover conditions which do not lead to the formation of tropical cyclones. At this stage, ~~it tends~~ these tracks are not to ~~shift up extreme values~~be considered as 'TCs tracks' but as 'candidate' tracks. In the following stage, TC tracks will be generated from candidate tracks by filtering those ones where meteorologiocal conditions for cyclone formation are satisfied.

Table A1. EM-DAT reporting proportions*

	Total Damages (US$)	Total Deaths	Insured (US$)	Total Affected	Recnst. Costs** (US$)
Ash fall	0,12%	1,09%	0,00%	0,09%	0,00%
Avalanche	0,02%	0,20%	0,02%	0,00%	0,00%
Coastal flood	0,30%	0,14%	0,14%	0,32%	0,00%
Cold wave	0,37%	0,70%	0,51%	0,25%	0,00%
Convective storm	9,86%	0,68%	21,78%	4,51%	0,00%
Drought	5,29%	24,75%	2,58%	36,35%	0,00%
Extra-tropical storm	1,60%	0,02%	3,09%	0,06%	3,31%
Flash flood	2,07%	2,58%	1,18%	3,03%	0,00%
Forest fire	2,45%	0,08%	3,86%	0,09%	0,76%
Ground movement	16,75%	26,78%	6,59%	2,61%	87,07%
Heat wave	0,68%	7,09%	0,03%	0,08%	0,00%
Land fire***	0,80%	0,03%	1,76%	0,02%	0,00%
Landslide	0,14%	1,04%	0,01%	0,15%	0,00%
Lava flow	0,02%	0,00%	0,00%	0,01%	0,00%
Mudslide	0,10%	0,21%	0,00%	0,02%	0,00%
Pyroclastic flow	0,01%	0,02%	0,00%	0,03%	0,00%
Riverine flood	16,61%	5,20%	6,59%	38,68%	4,46%
Rockfall	0,00%	0,02%	0,00%	0,00%	0,00%
Severe winter cond.	0,74%	0,16%	0,20%	1,27%	0,00%
Subsidence	0,00%	0,01%	0,00%	0,00%	0,00%
Tropical cyclone	**34,26%**	**18,33%**	**45,64%**	**12,34%**	2,23%
Tsunami	7,81%	10,87%	6,01%	0,11%	2,16%

Notes:

* Proportion exclude damages which sub types are not reported.

** Reconstruction costs are not well reported over disaster subtypes.

*** Brush, Bush, Pasture

Among disasters subtypes, tropical cyclones present an higher quality in reporting and represent a large share of total damages.